FINAL REPORT

Detection of Underwater UXOs in Mud

SERDP Project MR-2200

APRIL 2013

A.J. Hunter
R. van Vossen
B.A.J. Quesson
A.L.D. Beckers
TNO

SERDP
DOD ▪ EPA ▪ DOE

Contents

List of Figures

List of Tables

Acronyms

APL	Applied Physics Laboratory
BOSS	Buried Object Scanning Sonar
CMRE	Centre for Maritime Research and Experimentation
HF	High Frequency
LF	Low Frequency
MUD	Mine Underwater Detection
NRL	Naval Research Laboratory
NSWC-PC	Naval Surface Warfare Centre, Panama City
PHINS	Photonic Inertial Navigation System
REMUS	Remote Environmental Monitoring Units
RNLN	Royal Netherlands Navy
ROC	Receiver Operating Characteristics
RTK-GPS	Real Time Kinematic Global Positioning System
SAS	Synthetic Aperture Sonar
SERDP	Strategic Environmental Research and Development Program
SRR	Signal-to-Reverberation Ratio
TNO	Netherlands Organisation for Applied Scientific Research
UXO	Unexploded Ordnance

Keywords

Sonar, Synthetic Aperture Sonar, Interferometry, Wavelets

1 Abstract

a. Objectives: One of the most problematic areas where unexploded ordnance (UXO) can be situated is in an underwater environment, buried in sediment. Since burial frequently occurs in silt or mud, it is of great importance to have a capability for the detection of UXO in such buried conditions. This project considers detection of objects buried in mud using a side-looking low frequency (LF) sonar system mounted on a boat. The main advantage of such a system is that it has a wider area coverage compared to downward looking systems, enabling efficient surveying. The detection of buried UXO with a LF side-looking sonar system, however, is a challenging problem. This is primarily caused by high reverberation and possible clutter. In addition, the amplitude of the target echo of an object is reduced by burial. For these conditions, tools need to be developed for the detection of UXO and other targets of interest, and for the subsequent discrimination between targets and clutter contacts. It is critical that the processing and analysis techniques employed to achieve the task are evaluated on data acquired in operationally relevant conditions. The objective of this project is therefore to develop robust and advanced processing techniques for improving detection and classification in operational conditions, and to demonstrate these techniques on experimental data.

b. Technical Approach: To fulfil the objectives, the following processing techniques have been developed within this project:
   - Mitigation of multipath propagation in shallow water by exploiting the vertical receiver array
   - Synthetic aperture imaging including platform motion compensation
   - Fixed-focus SAS processing for resonating features
   - Enhance target-background separation (reverse SAS processing and shrinkage of incoherent wavelet coefficients
   - Multi-aspect acoustic colour extraction
   - Interferometric height estimation

   These techniques have been applied to data acquired with an experimental side-looking sonar system as part of a series of experiments funded by the Netherlands Ministry of Defense, and are used as input for this project. The experimental sonar system comprises both a horizontal and a vertical receiver array, enabling the signal to reverberation ratio to be improved by the suppression of multipath reverberation and to synthetically increase the aperture by synthetic aperture sonar (SAS) processing, and covers a bandwidth between 1 and 30 kHz. The data are acquired in the MUD2011 experiments conducted under operationally relevant conditions, in an estuary (Haringvliet) in the Netherlands. The water depth is in the range between 8 and 15 m with test objects such as sand-filled cylinders, boulders, 155-mm grenades, plastic targets, minelike targets and Mk82 and Mk84 bombs, both proud and buried.

c. Results: Towards developing a robust classification capability, we have demonstrated the extraction of multi-aspect acoustic colour from data collected by the MUD sonar in an operationally relevant environment. To achieve this, we have designed and implemented a processing chain aimed to optimally extract the multi-aspect target signature of resonating objects. It is demonstrated that the developed processing techniques mitigate perturbances introduced by platform motion errors and multi-path propagation, and that these enhance the signal-to-reverberation ratio. A number of different deployed targets have been analysed from data acquired in multiple runs. Observation of the corresponding

SAS images and multi-aspect acoustic colour plots indicate that these show similar patterns for repeated runs. Furthermore, distinguishing characteristics are observed that give reason to believe that robust classification is possible

d. Benefits: The way forward towards a capability for detecting and classifying buried objects is to improve the classification. Objects buried in mud can be detected, but the number of false alarms have to be reduced. To achieve this, robust features need to be identified to aid the classification. This would require the availability of a substantial amount of high-quality data with labelled objects, supported by high-fidelity modelling results. Because of the variability of acoustic colour, it is highly dependent on the environment and geometry, this is a challenging task. The benefits of this work are twofold:

   - Insight is provided on the information content that can be retrieved on resonating targets when data are acquired in operational settings.
   - Processing techniques are developed that aid the extraction of information on resonating targets.

   These are considered to be important steps towards the development of a capability to detect buried objects with a low false alarm rate.

2 Introduction

1.1 Background

High-frequency (HF) side-looking sonar (i.e., with frequencies higher than 50 kHz) is ideally suited to providing high-resolution images of the seabed. However, since sound does not penetrate into the seabed at these frequencies, HF systems cannot be used for the detection of buried objects, such as unexploded ordnances (UXOs). Low frequency (LF) side-looking sonar is a promising technology for the detection of objects buried in soft seafloor sediment. Acoustic energy is attenuated less by the sediment at lower frequencies and can therefore penetrate deeper, facilitating the detection of buried objects. Furthermore, a side-looking configuration yields a much higher area coverage rate compared to downward-looking systems (e.g., the BOSS system [5]) and this enables efficient surveys.

TNO have developed a broadband LF (1 kHz – 26 kHz) side-looking sonar for experimentation on buried object detection and, with funding and support from the Dutch Ministry of Defence, have conducted sea trials in relevant operational environments and conditions. The problem is difficult due to sea surface multipath reverberation in shallow waters and poor directivity at low frequencies, but these complications have been addressed by use of vertical array beamforming and synthetic aperture processing. Experimental results from the MUD-2009 and MUD-2011 sea trials demonstrate that objects buried in mud can be detected in data acquired by the MUD system [1],[2]. However, in practice it is a fundamental issue that, in addition to the targets of interest (e.g., UXOs), the system also observes *clutter* contacts, including other buried objects (e.g., boulders) and geological features below the mud (e.g., sand ripples). Therefore, a solution needs to be found for classifying the detections in order to discriminate between targets and clutter and thus suppress false alarms. This step is essential for the realization of an operational capability.

The LF and HF classification problems are fundamentally different. While information on size and shape derived from high-resolution images are commonly used for HF classification, these are not reliable for LF classification since the wavelength is on the same order of

magnitude as the dimensions of the objects of interest. However, structural resonances are generated in the objects at these frequencies and it is possible to exploit this. It has been indicated in experiments in controlled conditions and by modelling conducted by APL, NSWC-PC, and NRL, that useful information on the objects can be retrieved from their structural resonances [3],[4].

1.2 Objective

When a simple detection threshold is applied to LF-SAS images, the false alarm rate will generally be too high. More information is thus needed for constructing a detector with a sufficient probability of detection and an acceptable false alarm rate. The objective of the SERDP MR-2200 project is to work towards such a detector, i.e. to develop data processing techniques to optimally extract information on objects of interest from data acquired with an experimental LF-SAS system on data acquired in operationally relevant conditions.

To meet this objective, the following techniques have been implemented in a processing chain and applied to data from the MUD-2011 trial:

- Multipath mitigation in shallow water
- Synthetic aperture imaging including platform motion compensation
- Enhance target / background separation
- Multi-aspect acoustic colour extraction
- Interferometric height estimation

The results of this work provide valuable information for developing a robust data processing chain for broadband LF sonar systems. Furthermore, they are useful for exploring how the output can be exploited for improving detection and classification performance and assessing the added value in operationally relevant conditions.

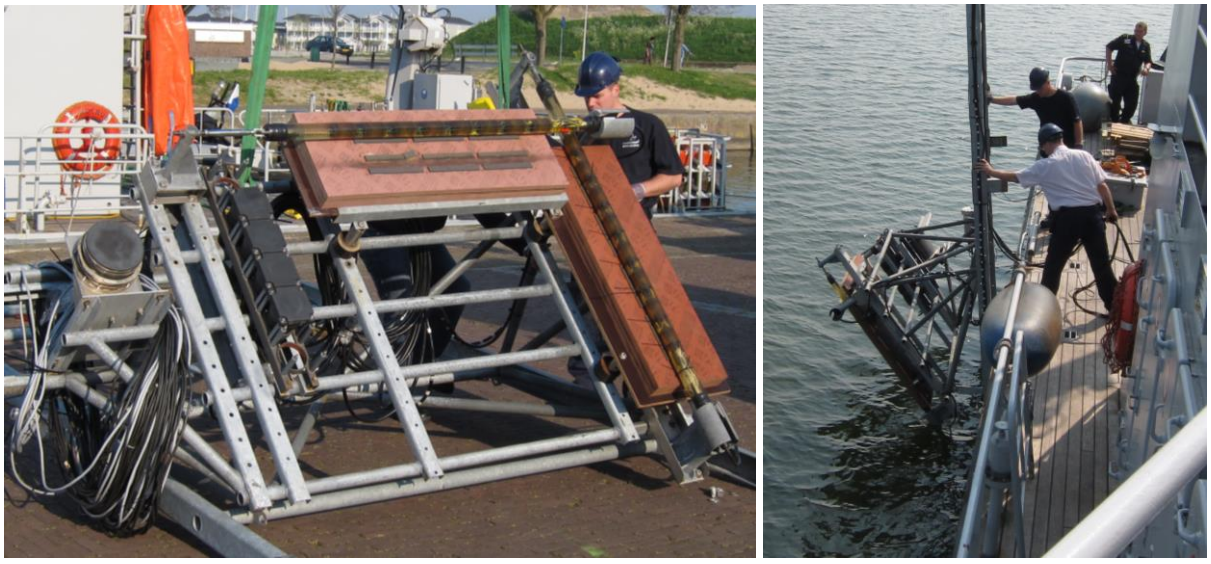

(a) (b)

Figure 1 – MUD system: (a) wet end; (b) deployment. Both the system depth and tilt angle can be modified, such that the system can operate in a water depth up to 30 m.

1.3 Outline of Report

The report is structured as follows: Section 2 provides an overview of the MUD system and the MUD-2011 sea trial, Section 3 describes the data processing chain and presents a selection of results, and Section 4 outlines the conclusions and way ahead. More detailed technical content and further results can be found in the appendices, where the various papers and presentations generated during the course of this work are included.

2 MUD System and 2011 Trial

The wet-end of the broadband LF sonar system is shown in Figure 1; it is comprised of an (exchangeable) acoustic source and two receiving arrays. Each array is composed of 16 hydrophones; one array is orientated vertically and the other horizontally. Three sources were available, covering the bandwidths from 1 kHz – 4 kHz, 4 kHz – 9 kHz, and 11 kHz – 26 kHz. The components are mounted on a frame that is adapted for operation from diver support vessels of the Royal Netherlands Navy (RNLN). Both the depth of the transducers and the tilt angle of the frame can be modified. With the current system settings and processing, the system can be used up to 30 m water depth.

Two navigation sensors are used to monitor the position and orientation of the sonar system; these are located on top of the support frame. An inertial navigation system (PHINS), records the 3-D accelerations and rotation angles of the system, and a real time kinematic global positioning system (RTK GPS) provides centimetre positioning accuracy. These non-acoustical systems are necessary in order to derive the exact position and orientation of the system with respect to the test area. This accurate navigation is also required for more advanced signal processing, and in particular for synthetic aperture sonar (SAS) processing.

For the population of the test garden, a selection was made from a range of objects with different characteristics: mine-like and non mine-like, UXOs, ferromagnetic, and other materials and different shapes. These targets were distributed over three lines in the test garden, with an average distance between targets of approximately 25 m. The test garden was deployed 6 months before the trial. The water depth in the trial area is in the range between 8 and 15 m.

The MUD-2011 trial took place from 18 April 2011 to 22 April 2011. In this period, a total of 220 runs were executed covering different parts of the test garden. REMUS control runs were conducted in February 2011 and during the trial in April 2011.

3 Data Processing Chain and Algorithm Improvements

The objective of the processing is to prepare the received data for optimal extraction of information for classification (i.e., features). Here, the focus is on the retrieval of multi-aspect acoustic colour since previous work has indicated that useful features relating to the structural resonances can be derived from this information [4]. Interferometric processing has also been investigated for obtaining the seafloor bathymetry and object heights, which may provide useful information on the objects and environment.

In operational conditions, the processing is not straightforward due to multipath propagation in shallow water and deviations from a nominally straight trajectory [8].

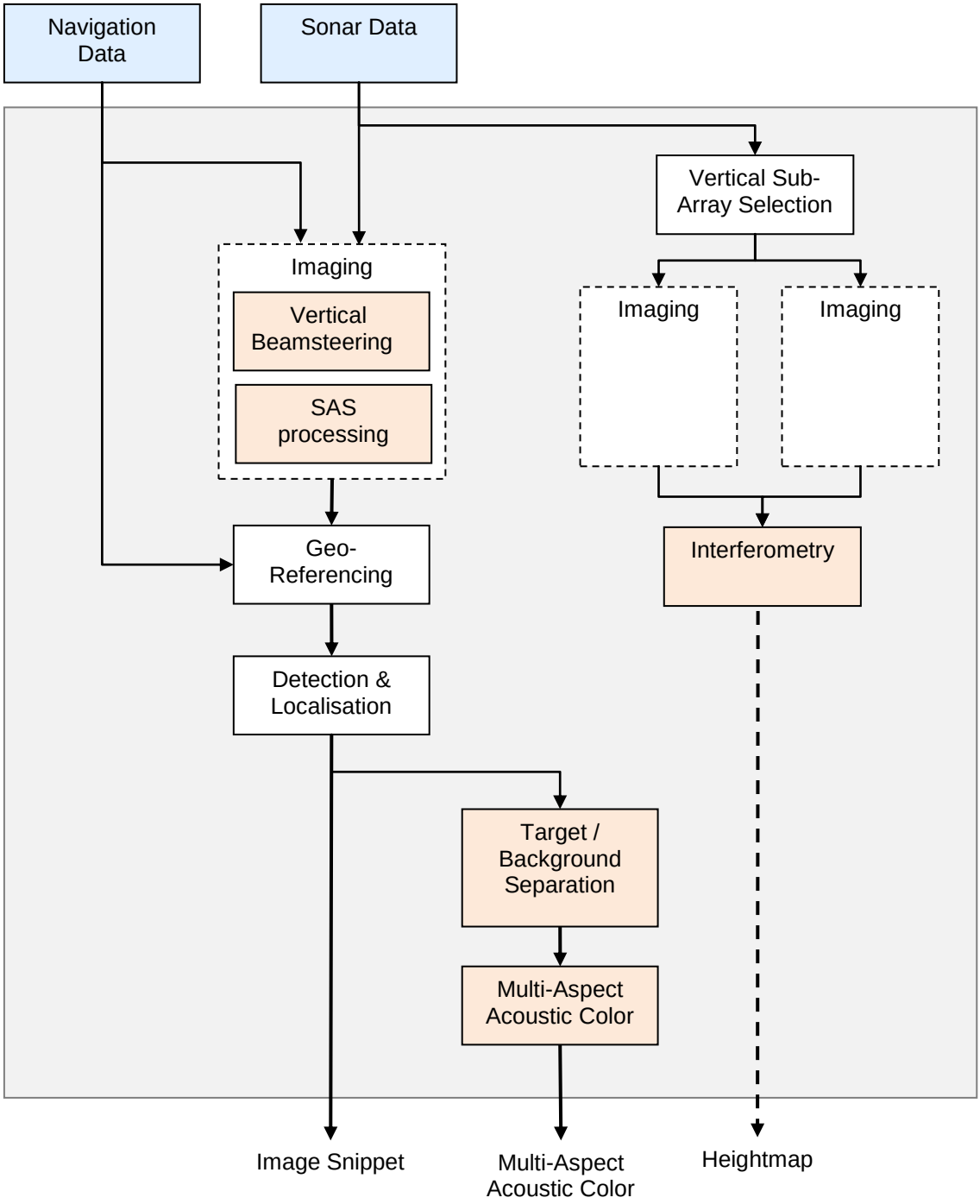

Figure 2 – Data flow diagram for the MUD processing chain. The processing represented within the orange boxes is explained in more detail in this report.

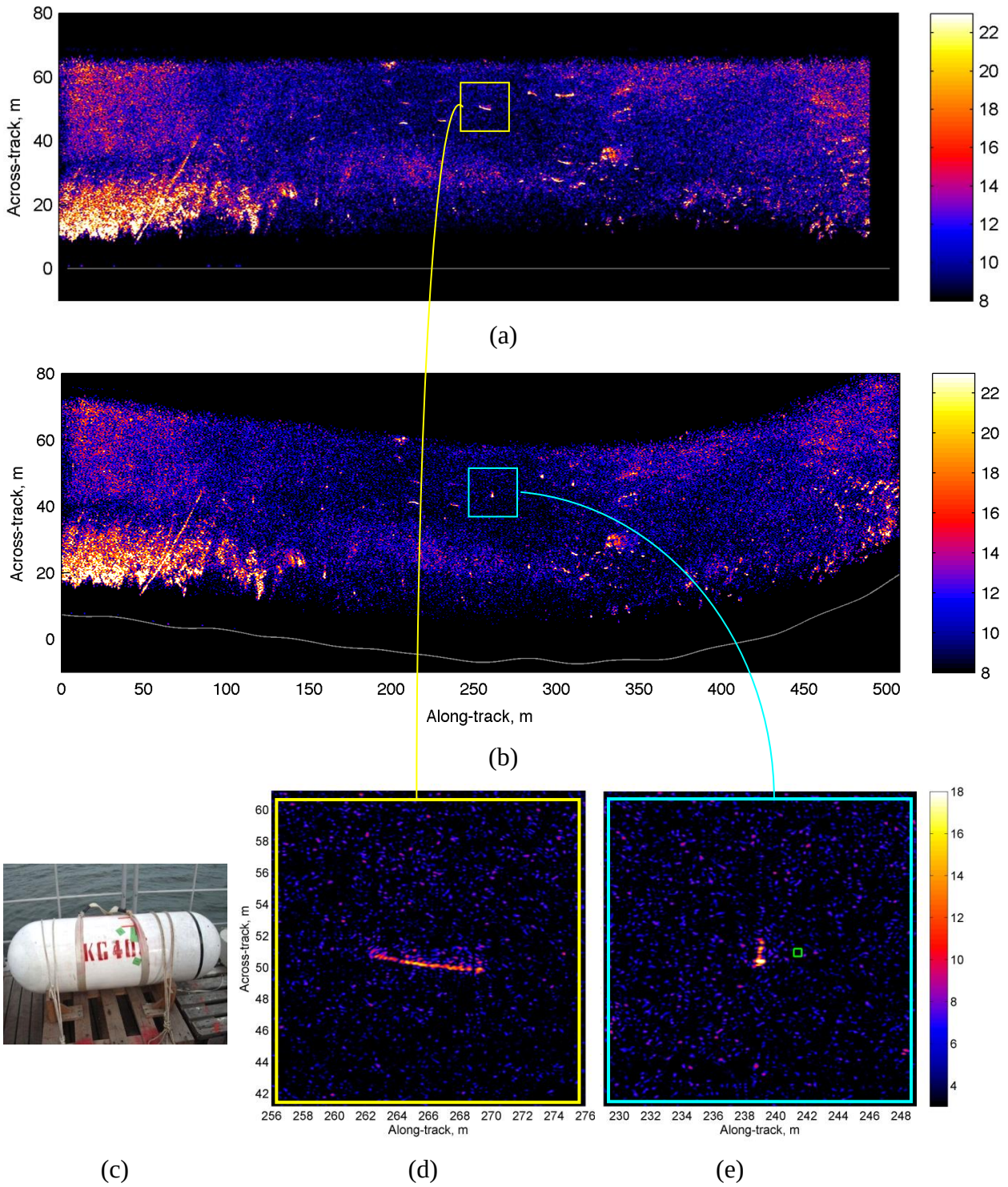

Figure 3 – Broadband low frequency SAS imagery of run 275 (a) without and (b) with widebeam motion compensation, where the gray curves show the assumed and measured sonar paths, respectively; (c) the CMRE EVA cylinder, and corresponding image snippets (d) without and (e) with motion compensation, where the green marker indicates the deployment ground-truth location. The water depth is in the range between 8 and 15 m.

Therefore, the processing needs to be capable of dealing with these issues in order to robustly retrieve information on the targets.

The processing chain is outlined in Figure 2. In this section, the key stages of the chain and improvements to the algorithms are described. It should be noted that all processing steps, except vertical array beam-steering and interferometry, are generally applicable to SAS systems. In shallow water, the vertical processing is important because it mitigates image degradation caused by multipath propagation. Some examples from the MUD data are presented as illustrations, and further results and technical details can be found in the Appendices. Specifically, Appendix B provides a complete and detailed technical description of the processing chain and a selection of results from a variety of deployed objects and runs.

3.1 Widebeam Vertical Beamsteering

In shallow waters, multipath reverberation can obscure or corrupt the echoes from targets. This has a negative impact on detectability and the quality of derived information (e.g., multi-aspect acoustic colour), particularly at longer ranges. The MUD system has a vertical array of 16 hydrophones, which allows beamsteering towards the seafloor for receiver-side multipath mitigation. However, a drawback of using the vertical array (compared to the horizontal array) in the MUD system is that it results in sparse spatial sampling of the synthetic aperture and the introduction of aliasing artefacts in the imagery. Regardless, the multipath reverberation was found to be much more problematic than the aliasing artefacts which are somewhat diminished by the broad bandwidth. For this reason, we focused on data from the vertical array only.

Initially, multipath mitigation was achieved by performing SAS processing on data from each of the hydrophones independently and then forming the vertical beam from the focused SAS images, as described in Appendix C. However, this procedure makes an implicit assumption of a narrow horizontal beam, which is not the case. An improvement to the procedure has since been made to accommodate the wide horizontal beam. The vertical beamforming is instead performed before the SAS processing and compensations are made for the aspect-dependent changes in the elevation angle to the seafloor; this is described in Appendix B. This improved procedure results in better suppression of the multipaths at wide angles.

3.2 Synthetic Aperture Sonar (SAS)

The sidescan echo data from the MUD system has very poor resolution due to its wide horizontal beams. Therefore, synthetic aperture sonar (SAS) processing is essential for achieving sufficient resolution so that the target responses can be isolated from other nearby contacts and the background reverberation. This is very important for subsequent analysis of the target response (e.g., multi-aspect acoustic color). Furthermore, SAS processing significantly enhances the signal-to-reverberation ratio (SRR), improving detection performance, and is essential for achieving sufficient resolution to allow interferometric processing.

3.2.1 Widebeam Motion Compensation

Uncompensated deviations from a nominally straight trajectory can cause corruption of the SAS imagery, reducing SRR and introducing blurring and image artefacts; this is illustrated in Figure 3. Deviations from a straight path are unavoidable in operational conditions, since this requires 2-4 cm navigation accuracy ($\lambda/10$ in the 4-9 kHz band, where λ denotes the wavelength), and, therefore, must be compensated to ensure a high quality input

to the follow-on processing. This requirement is relaxed after the application of motion compensation. It is required that the sailed track can be resolved in post-processing with 2-4 cm accuracy instead.

A Fourier-domain algorithm (referred to in the literature as either the wavenumber, omega-k, or Stolt migration algorithm) [10] was used initially to perform the SAS processing of the MUD data. The sonar trajectory was measured using RTK GPS. However, motion compensation is not straight-forward in the Fourier domain due to the wide horizontal beams and an approximate solution was used to compensate the SAS image snippets (see Appendix C). Since then, a back-projection algorithm [11] has been implemented, facilitating approximation-free wide-beam motion compensation for the entire image (see Appendix B). To make the best use of the broad bandwidth, the algorithm is applied for multiple sub-bands with optimal angular filtering in each band.

Figure 3(b) shows an example motion-compensated SAS image from a run in the MUD-2011 trial using the 4 kHz – 9 kHz acoustic source. Many well-focused contacts that correspond to the deployed objects and seabed structures can be observed. High SRR target responses can be observed up to ranges of at least four times the water depth. One can also observe multipath replicas behind some of the high SRR targets at long ranges and this is caused by the source-side multipath modes, which cannot be mitigated by receiver-side beamsteering [12].

In addition to the deployed targets within the footprint (all of which were observed), there are many unidentified clutter contacts; these are thought to be other objects and / or seafloor features. Based on the large number of clutter contacts, it is clear that dealing with false alarms is a very relevant issue. For targets located in high-clutter area, detection is not considered to be feasible without additional information. Based on this observation, one can conclude that confident detections cannot be made based on thresholding an LF-SAS image, and that additional information has to be used. Techniques developed within the SERDP MR-2200 project are discussed in the following sections.

3.2.2 Fixed-Focus Resonance Enhancement

In standard SAS processing, each image pixel is assumed to correspond to a unique location on the seafloor and a geometrical argument is made to determine the corresponding locus of echoes in the data. However, this assumption is violated for resonant scattering since the resonant echoes originate from the location of the object but manifest in the data at longer ranges. The loci of resonances do not exhibit the assumed curvature and are thus defocused by standard SAS processing. For a resonant object at a known location, it is better to focus the resonant "tail" using modified focal laws based on the range of the target instead of the pixel. This is termed *fixed-focus SAS* and it has been used previously for target shadow enhancement based on a similar principle (i.e., the shadow originates from the target location but manifests in the data at longer ranges) [13].

Fixed-focus SAS processing was applied to resonant targets in the MUD data and found to enhance the resonant response, as demonstrated in Figure 4, where the observable tail extends to approximately 2m of range in the standard SAS image but up to 3m in the fixed-focus image; in this case, the improvement equates to a 50% increase in the measureable resonant response.

3.3 Target / Background Separation

SAS processing is essential for achieving sufficient resolution to reliably separate targets from other nearby contacts and the background reverberation. Initially, the separation was

achieved by a simple windowing of the SAS image, as described in Appendix C. However, this is sensitive to the choice of window; a smaller window achieves better suppression of the background but at the risk of losing important information on the target, especially the resonances.

An improved method has been developed that computes a metric for the multi-look image coherence and uses a threshold to distinguish between targets and background under the assumption that coherent regions of the image correspond to the target whereas incoherent regions correspond to the background. Computation of the coherence metric and the thresholding operation is performed in the wavelet domain to take advantage of the sparsity in this domain. A demonstration of the target / background separation is shown in Figure 4 and Figure 5. A more detailed description of the incoherent wavelet shrinkage method and further results can be found in JASA paper (submitted for review) in Appendix A, where an average 15-20 dB improvement in signal-to-reverberation ratio is demonstrated.

3.4 Multi-Aspect Acoustic Colour

SAS imagery contains important phase information that can be used to derive useful information, such as aspect and frequency-dependent scattering characteristics, i.e., the multi-aspect acoustic colour. This is especially relevant for broadband LF data, in the frequency range in which resonances occur. The following approach is used to extract the multi-aspect acoustic colour of a target:

- The contact corresponding to the deployed object is selected in the geo-referenced SAS image using navigation data and ground truth information on the object deployment locations.
- The target is isolated from the background reverberation in the SAS image snippet by application of the incoherent wavelet shrinkage technique of Appendix A.
- The image of the isolated target is Fourier transformed to the wavenumber domain.
- A coordinate transform from wavenumber to angle is performed to obtain the aspect versus frequency representation.

A detailed technical description and illustration of these steps is given in the Appendices. It is important to emphasize that robust extraction of the multi-aspect acoustic colour relies not only on the careful implementation and execution of these steps, but also the quality of the SAS image.

An example multi-aspect acoustic colour measurement of a buried cylindrical object (see Figure 3(c)) is shown in Figure 6. Figure 6(a) and (b) show the measurements from two independent runs with similar trajectories, demonstrating the repeatability of the results. This particular target exhibits a strong response at an angle of approx. 30deg, indicating the orientation of its axis of symmetry relative to the track. It also exhibits a strong modal response over the frequency range, which could be indicative of structural resonances. In Figure 7, the SAS image snippets and multi-aspect acoustic colour measurements from multiple runs with different headings and stand-off distances (i.e., elevation angles) are combined in one multi-dimensional representation. This fusion of information provides a scattering “fingerprint” for the target from which it might be possible to derive robust classification features.

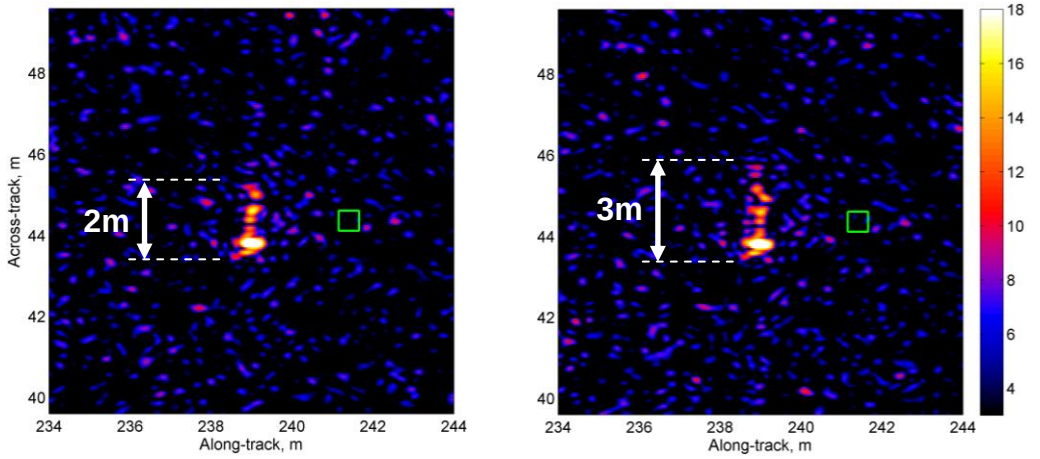

(a) (b)

Figure 4 – SAS image snippets of the CMRE EVA cylinder using (a) regular processing; and (b) fixed-focus processing, demonstrating improved focusing of the resonant "tail".

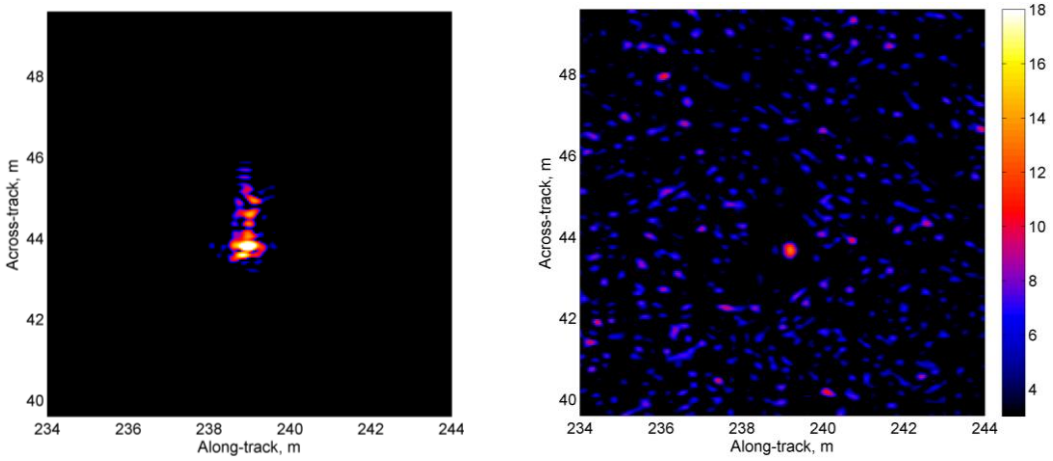

(a) (b)

Figure 5 – Separation of (a) the coherent target response from (b) the incoherent background reverberation using the incoherent wavelet shrinkage technique.

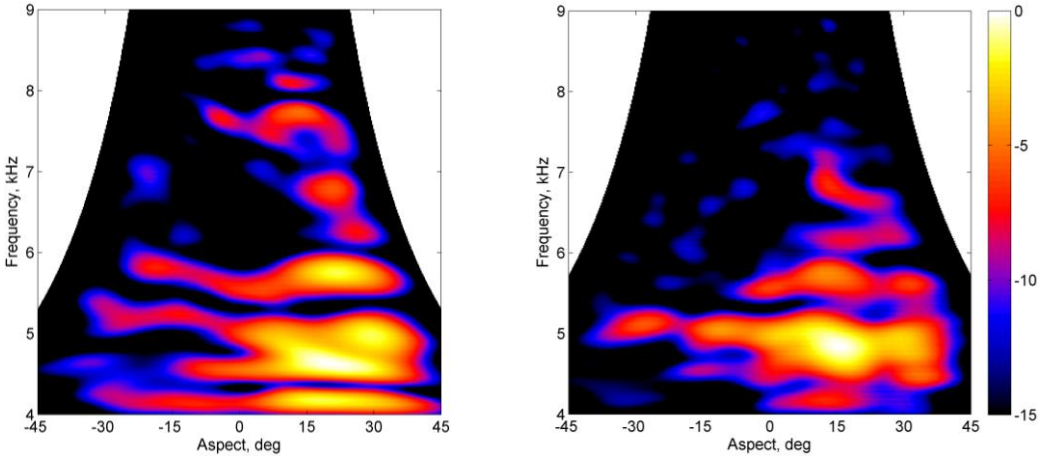

(a) (b)

Figure 6 – Extracted multi-aspect acoustic colour of the CMRE EVA cylinder from different runs with similar geometries: (a) run 325 and (b) run 275.

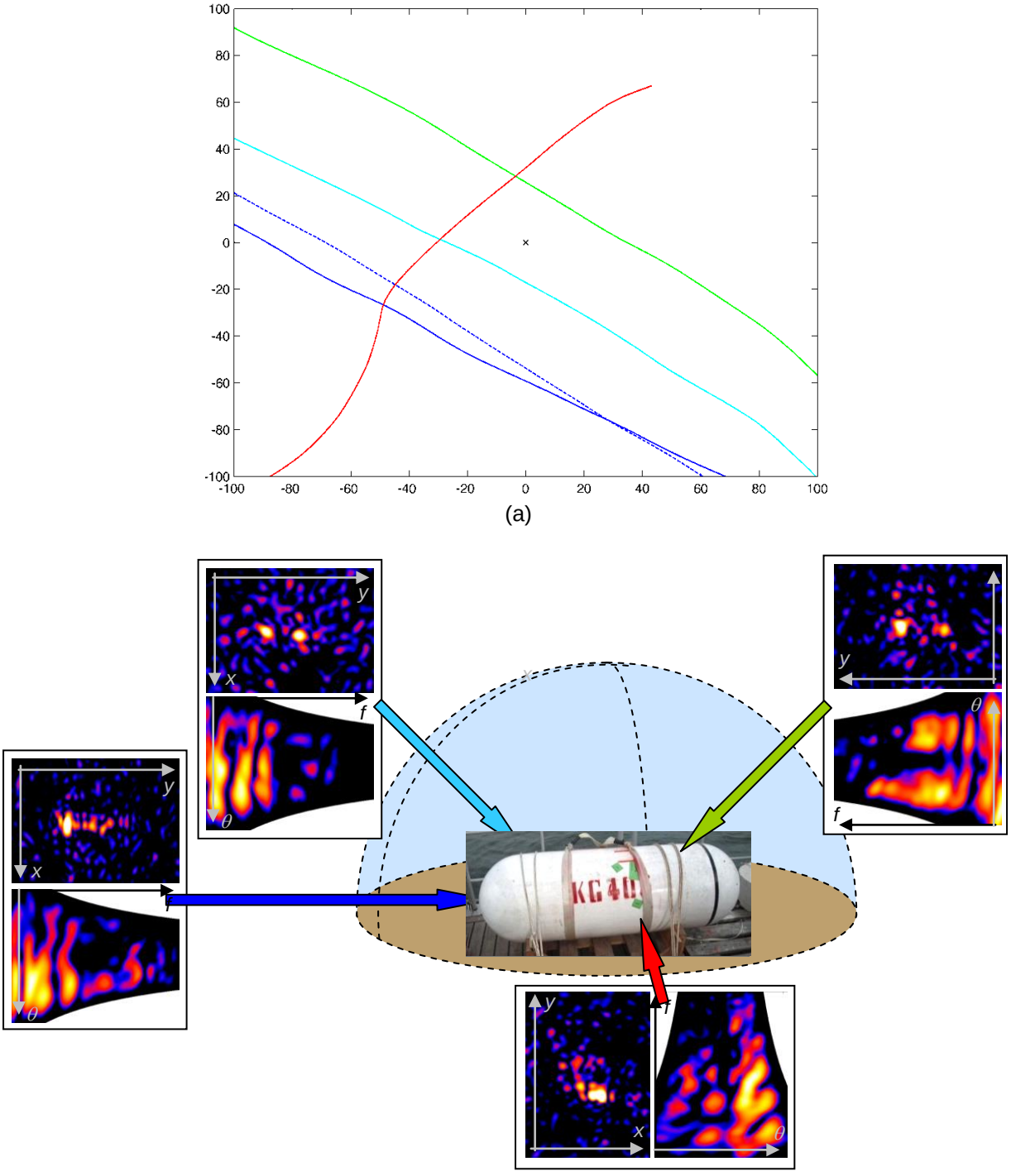

Figure 7 – SAS image snippets and multi-aspect acoustic colour plots from multiple runs of different geometries. The image snippets show an area of 5x4 m around the target, and the acoustic colour plots show dependencies in aspect angle from -45 to 45 deg relative to broadside and frequencies from 4 to 9kHz.

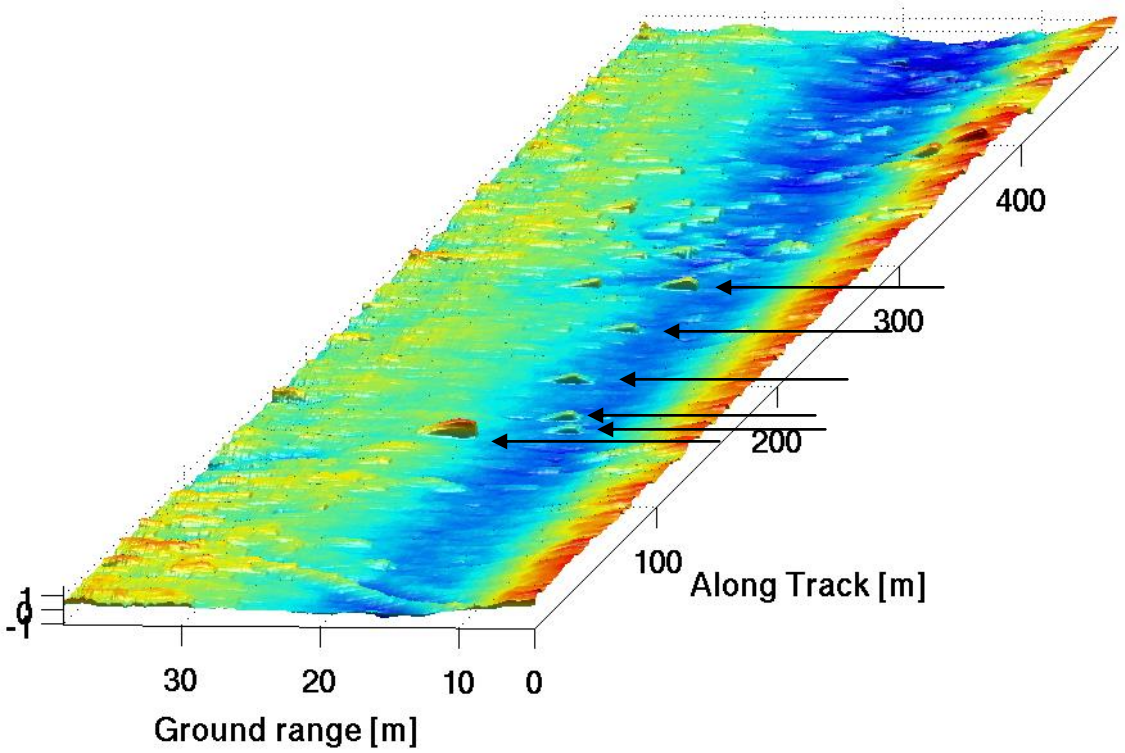

Figure 8 – Interferometric heightmap from run 325. The arrows indicate deployed objects, which clearly are above the mud-sand interface. The water-mud interface appears to be acoustically transparent in the LF frequency range.

SAS images and multi-aspect acoustic color plots of a variety of different objects are given in the Appendices. It is apparent from these results that different objects do exhibit some pronounced differences and that these differences could be exploited for classification.

3.5 Interferometry

Interferometric processing is commonly used on high-frequency SAS data to infer information on the bathymetry and on the height of objects [6]. For LF data which penetrates into the seabed, it is not necessarily information on the bathymetry that will be retrieved. The height information that is obtained corresponds to the most dominant scatterer within a resolution cell, and this could also be a subsurface structure.

The vertical array of the MUD system can be divided into smaller sub-arrays for interferometric processing. Each sub-array is steered towards the seafloor for multipath suppression (with reduced performance due to the smaller sub-array dimensions); SAS images are generated and co-registered; and the phase differences between the SAS images are computed and converted to a height map. An example height map is shown in Figure 8, where the useable swath has been reduced to 40m due to the poorer multipath suppression. The nominal depth of the background reverberation is approximately 1 m deeper than the known water depth, suggesting that the background reverberation is from a sand interface below the mud layer. The contacts observed in the SAS images are also observed in the height map and they exhibit greater heights than the background reverberation from the sand-mud interface. As a result, interferometry could also contribute to separating large objects from clutter contacts.

4 Discussion

In the current project, processing techniques have been developed for LF-SAS data acquired with a ship-mounted system. Because the tilt angle of the system can be modified, the system can provided images up to 30 m water depth. To meet the navigation requirements for SAS, the ship's track is resolved using RTK-GPS data.

For application in larger water depths, the current system is not a viable solution, and AUV-mounted solutions should be considered instead. To meet the navigation requirements, the track has to be resolved by combining INS and data-driven techniques, since GPS data are not available then. Note as well that the bulky vertical array is not needed as well in this situation, since multipath propagation only needs to be mitigated in shallow water (< 30 m). All processing techniques developed in this project are also applicable to these AUV-mounted solutions, except the vertical array beamforming and interferometry.

Some limitations of the MUD system have been identified as well. Due to the directivity pattern of the low-frequency transducers, multipath is still an issue. Furthermore, there are aliasing issues in the along-track direction. As a consequence, only a limited portion of the MUD data could be included in the analysis.

The multi-aspect acoustic color results suggest that interesting features extend beyond the 4-9 kHz bandwidth that is used in the current analysis. Modeling studies support this observation. In future experiments, we intend to examine larger bandwidth. Especially the lower frequencies are of interest, because it is anticipated that these excite strong resonances that could be a useful feature for detection and classification.

5 Conclusions

Using TNO's MUD low frequency broadband sonar (in the frequency band 4–9 kHz), we have demonstrated the capability to observe high SRR target responses for a variety of objects including UXOs buried in mud. Furthermore, this was achieved at a high mapping rate of approx. 0.5 km/h due to the sidescan imaging geometry compared to downward-looking systems. However, many unidentified clutter contacts were also observed in the imagery, highlighting a potential shortfall and the need for a capability to classify contacts.

Key modifications of processing chain	**Benefits**
Wide-beam vertical beam-steering	Multi-path suppression
Wide-beam motion compensation and broadband back-projection SAS	Critical for deriving multi-aspect acoustic colour information (Figure 3); compensates for artefacts introduced by residual motion errors
Fixed-focus synthetic aperture imaging	Enhancement of resonant targets (Figure 4)
Incoherent wavelet shrinkage technique	10-15 dB enhancement of signal-to-reverberation ratio (Figure 4 and Figure 5)
Reverse synthetic aperture processing	Extract multi-aspect acoustic colour information (Figure 6 and Figure 7)
Interferometric processing	Possible clues on classification and burial depth

Table 1 – Key modifications of processing chain to enable the extraction of robust features.

Towards developing a robust classification capability, we have demonstrated the extraction of multi-aspect acoustic colour from data collected by the MUD sonar in an operationally relevant environment. To achieve this, we have designed and implemented a processing chain and made improvements to our algorithms. The key aspects are listed in Table 1. In addition to the extraction of multi-aspect acoustic colour information, these aim to enhance the SRR and to resolve artefacts introduced by residual motion errors.

A number of different deployed targets have been analysed from data acquired in multiple runs. Observation of the corresponding SAS images and multi-aspect acoustic colour plots indicate that these show similar patterns for repeated runs. Furthermore, distinguishing characteristics are observed that give reason to believe that robust classification is possible (Appendix C).

6 Way Ahead

The SAS images obtained in the MUD-2011 experiment indicate that it is not possible to have a good detection performance by simply applying a detection threshold. Not only deployed targets have a high SRR, but also clutter contacts caused by seafloor features and other objects. This generally results in an excessive false alarm rate for an automated detector. Furthermore, LF-SAS images are generally too complex for a human operator. In our opinion, more information should therefore be used for the detection process. In the current project, strategies have been developed to optimally extract this information. As a way forward, we propose a two-stage detection process that uses this additional information:

1) Identify areas in which coherent scattering occurs. This is a detector for both targets and clutter, and serves as a first filter to reduce the amount of data. We suspect that it is feasible to develop such a detector based on the technique presented in Appendix A.
2) Investigate these contacts by using a classifier, with the objective to distinguish man-made objects from clutter. In the current project, processing techniques have been developed that aim to optimally extract additional information on contacts, such as multi-aspect acoustic color information with structures from resonances preserved. In follow-on work, a classifier that distinguishes man-made objects from clutter would need to be developed. This involves the selection of suitable features, and the interpretation by a human operator, and the implementation into a classifier.

Once such a classify-before-detect approach has been developed, the detection performance needs to be evaluated (both probability of detection and false alarm rate) and quantified using receiver-operating-characteristics (ROC) curves. This performance should be evaluated on different data sets, and compared to the performance of a human operator.

To aid the development of a robust classify-before-detect approach, the optimum bandwidth should be selected. In the current project, we analysed data in the 4-9 kHz frequency band. Both modelling studies and also the multi-aspect acoustic color images indicate that it should be considered to extend this bandwidth to both lower and higher frequencies. Then, more information is available on both targets and clutter contacts, and a better discrimination should become feasible.

7 List of Publications

1. A.J. Hunter and R. van Vossen, "Sonar target enhancement by shrinkage of incoherent wavelet coefficients, submitted to JASA-EL, 2013. [Appendix A]
2. A.J. Hunter, R. van Vossen, B.A.J. Quesson, A.L.D. Beckers, "Acoustic signatures of underwater UXO measured by low frequency broadband SAS", to be submitted to Underwater Acoustic Conference (UAC), Corfu, Greece, 2013. [Appendix B]
3. A.J. Hunter, R. van Vossen, B.A.J. Quesson, M.E.G.D. Colin, M. Zampolli, A.L.D. Beckers, "Low frequency synthetic aperture sonar for detection and classification of buried objects", European Conference on Underwater Acoustics (ECUA), Edinburgh, 2012 [Appendix C]
4. A.J. Hunter, "Tutorial on ultra-low frequency wideband and widebeam sonar processing, ONR iSAAM Workshop, 2012. [Appendix D]

References

[1] A.L.D. Beckers, R. van Vossen, S.P. Beerens, B.A.J. Quesson, M. Zampolli, J.C. Sabel, J. Janmaat, "Mud trial final report", TNO-DV 2010 A004, 2010.

[2] A.L.D. Beckers, B.A.J. Quesson, R. van Vossen, "MUD Trial Phase 2 – Final Report", TNO-DV 2011 A343.

[3] J.A. Bucaro, B.H. Houston, M. Saniga, L.R. Dragonette, T. Yoder, S. Dey, L. Kraus, and L. Carin, "Broadband acoustic scattering measurments of underwater unexploded ordnance (UXO)", Journal of the Acoustical Society of America, 123, 738-746, 2008.

[4] K.L. Williams, S.G. Kargl, E.I. Thorsos, D.S. Burnett, J.L. Lopes, M. Zampolli, P.L. Marston, "Acoustic scattering from a solid aluminum cylinder in contact with a sand sediment: Measurements, modeling, and interpretation", Journal of the Acoustical Society of America 127, 3356-3371 2010.

[5] S.G. Schock, A. Tellier, J. Wulf, J. Sara, M. Ericksen, "Buried object scanning sonar", IEEE Journal of Oceanic Engineering, 26, 677-,689 2001.

[6] T.O. Saebø, R.E. Hansen, A. Hanssen, "Relative height estimation by cross-correlating ground-range synthetic aperture sonar images", IEEE Journal of Oceanic Engineering 32, 971-982, 2007.

[7] T.M. Marston, P.L. Marston, K.L. Williams, "Scattering resonances, filtering with reversible SAS processing, and applications of quantitative ray theory", OCEANS 2010, 1-9, 2010.

[8] A. Bellettini and M.A. Pinto, "Theoretical accuracy of synthetic aperture sonar micronavigation using a displaced phase-centre antenna", IEEE Journal of Oceanic Engineering 27, 780-789, 2002.

[9] A. Tesei, M. Zampolli, G. Canepa, "At-sea measurements of acoustic elastic scattering by a 1.5 m long cylinder made of composite materials", 2nd International Conference on Underwater Acoustic Measurements, Crete, Greece, 2007.

[10] P.T. Gough and D.W. Hawkins “Imaging algorithms for a strip-map synthetic aperture sonar: minimizing the effects of aperture errors and aperture undersampling”, IEEE Journal of Oceanic Engineering, 22(1), 1997

[11] R.E. Hansen, “Introduction to synthetic aperture sonar”, Sonar Systems, InTech, 2011.

[12] M.P. Hayes and A.J. Hunter, “Adaptive beamforming for low frequency SAS imagery and bathymetry”, European Conference on Underwater Acoustics (ECUA), Edinburgh, 2012

[13] J. Groen, R.E. Hansen, H.J. Callow, J.C. Sabel, T.O. Saebø, “Shadow enhancement in synthetic aperture sonar using fixed focusing”, IEEE Journal of Oceanic Engineering 34, 269-284, 2009.

Appendix A Article on Target Response Isolation

(Submitted to JASA-EL)

Sonar Target Enhancement by Shrinkage of Incoherent Wavelet Coefficients

A. J. Hunter and R. van Vossen

TNO (Netherlands Organisation for Applied Scientific Research),

Oude Waalsdorperweg 63, 2597 AK The Hague, The Netherlands

alan.hunter@tno.nl, robbert.vanvossen@tno.nl

Abstract

Background reverberation can obscure useful features of the target echo response in broadband low-frequency sonar images, adversely affecting detection and classification performance. This letter describes a phase and resolution -preserving means of separating the target response from the background using a coherence-based wavelet shrinkage method proposed recently for de-noising magnetic resonance images. The algorithm weights the image wavelet coefficients in proportion to their coherence between different looks under the assumption that the target response is more coherent than the background. The algorithm is demonstrated successfully on experimental synthetic aperture sonar data from an operational broadband low-frequency sonar developed for buried object detection.

PACS: 43.60.Hj

1. Introduction

Broadband low-frequency sonar is a promising technology for the robust detection and classification of objects that are proud of or buried beneath the seafloor. While conventional high-frequency imaging sonar relies on geometrical features (such as the highlights and shadows) to detect and classify objects, broadband low-frequency sonar can be used to exploit structural resonances of the objects [1,2]. The classification of contacts in broadband low-frequency sonar imagery thus depends on a capability to reliably extract the resonant echo response. In practice, the echo response is corrupted by background reverberation adversely affecting this capability. This is a problem for low-frequency sediment-penetrating sonars, e.g., the TNO MUD [3], SSAM [4], and BOSS [5] systems, where the seafloor sediment and / or multipath reverberation can be strong while useful features of the echo response can be comparatively weak.

Synthetic aperture sonar (SAS) processing provides increased image resolution by exploiting the inter-ping phase coherence of the echo data. Furthermore, it enhances the signal-to-noise ratio for coherent targets relative to the incoherent background reverberation [6]. Use of a directional source and / or receiver array can further mitigate the multipath reverberation in shallow water [7]. However, even with these mitigation measures in place, the residual reverberation can be problematic.

A target's multi-aspect acoustic colour and the echo response from which it is derived are useful representations for classifying targets in low-frequency broadband sonar data [8]. The target response can be isolated from the background reverberation in the SAS image by spatial filtering (i.e., by windowing the target so that nearby scatterers and reverberation are removed)

followed by reverse SAS processing [8,9]. However, there is a trade-off for the choice of filtering bandwidth; a smaller window achieves greater suppression of the reverberation but at the cost of reduced spatial frequency resolution. Furthermore, any reverberation remaining within the window is retained.

Ideally, the reverberation would be removed without sacrificing spatial frequency resolution; a novel wavelet shrinkage method was proposed recently for de-noising magnetic resonance images [10,11] that is capable of achieving this. In this letter, we adapt this method for the purpose of separating coherent targets from the incoherent background reverberation in SAS images whilst preserving the phase structure and retaining a high resolution. We demonstrate application of the method on experimental data from the TNO MUD low-frequency sediment-penetrating sonar.

2. Algorithm Description

The wavelet shrinkage method uses a coherence metric to determine the similarity of wavelet coefficients between independent looks, i.e., different images of the same scene with statistically independent noise realisations. The wavelet coefficients that have high coherence between looks are assumed to correspond to the reverberation-free measurements of the targets, whereas the coefficients with low coherence are assumed to correspond to the reverberation. Under these assumptions, the coefficients with low coherence are attenuated to produce a de-noised image. The adaptation of this method to the sonar application is described in the following sections and is summarised in Figure 1.

2.1. Generation of complimentary looks

In the context of target detection and classification for broadband low-frequency sonar, the major source of interference is from the seafloor sediment and multipath reverberation. Here, we assume that the reverberation cannot be resolved by the system and, therefore, behaves as speckle, i.e., it has low coherence over the spatial and temporal frequencies [12]. Comparatively, targets are assumed to be much more coherent. These are the characteristics of the data that are exploited to generate statistically independent looks.

A broadband low-frequency synthetic aperture sonar collects samples over a wide range of temporal and spatial frequencies due to the use of a broadband pulse and wide beams, respectively. Therefore, the SAS echo data have broad support in the wavenumber domain. Complimentary looks can thus be generated by partitioning this space into two sets.

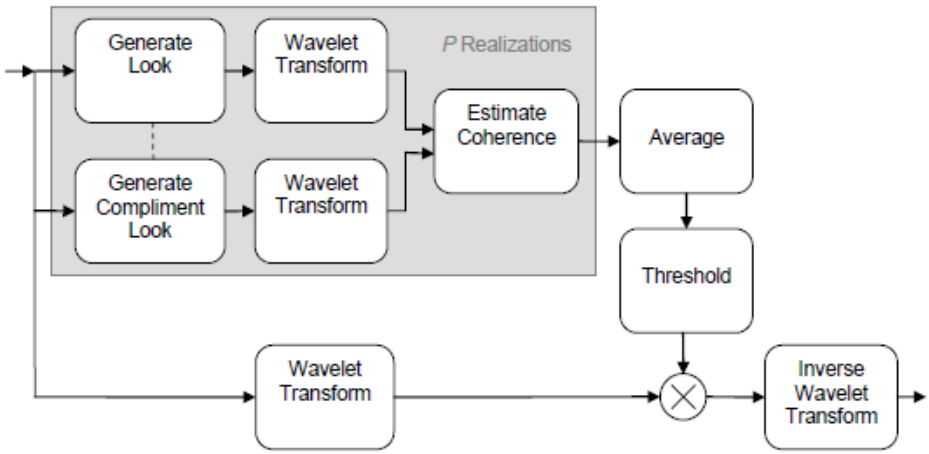

Figure 1 – Overview of the wavelet shrinkage algorithm.

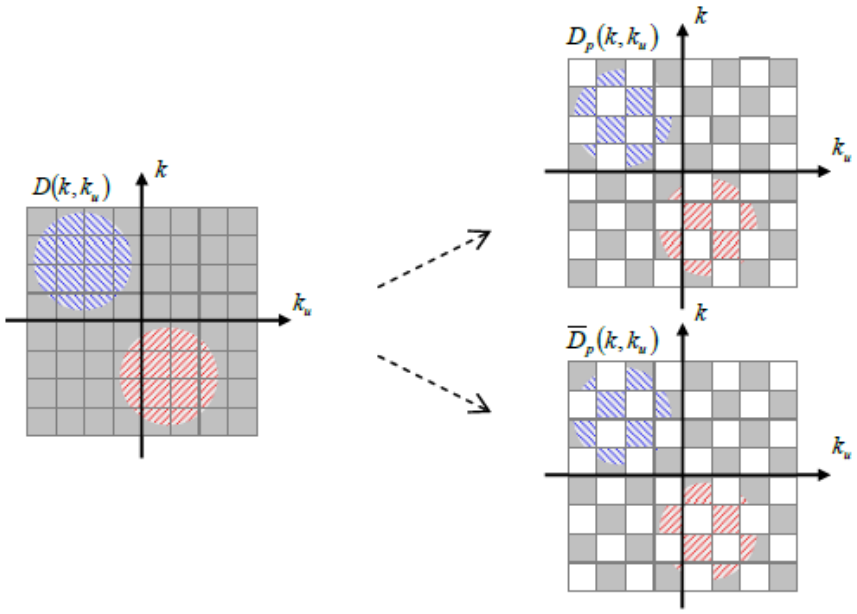

Figure 2 – Generation of complimentary looks by a regular partitioning of the wavenumber space where alternate blocks are assigned into two sets. The hashed areas represent regions of the space corresponding to target responses that are correlated over multiple blocks.

The partitioning of wavenumber space must be made so that this relationship is preserved in order to exploit the assumed coherence of the target and relative incoherence of the background. One means of achieving this is to apply a 2-D grid to the space and assign blocks to either one or the other set; this is illustrated in Figure 2 for a regular assignment between sets. It is necessary to choose a grid such that the speckle is correlated only on a scale that is much smaller than the block size and the target is correlated on a scale that is bigger. In this way, the targets are likely to retain coherence between the blocks whereas the speckle is not. The derivation of an optimal grid will depend on the assumed scattering properties of the targets and reverberation, and the system parameters; this is an interesting subject for future research but is not considered here.

Often in practice, the data are sampled at close to the Nyquist rate or perhaps even under-sampled and a regular separation of blocks between sets (as illustrated in Figure 2) can result in under-sampling and the introduction of artefacts. In these cases it is advantageous to partition the space using a randomised assignment between sets, thus breaking the regularity and spreading the energy of the under-sampling artefacts rather than concentrating them into localised grating lobes. Here, we use a randomised partitioning scheme where blocks are assigned to either of the two complimentary sets (looks) at random, i.e.,

$$D_p(k,k_u) = D(k,k_u)\mathrm{w}_p(k,k_u)$$

$$\overline{D}_p(k,k_u) = D(k,k_u)\left[1-\mathrm{w}_p(k,k_u)\right],$$

where $D(k,k_u)=\mathrm{FT}\{d(t,u)\}$ is the 2-D Fourier transform of the echo data $d(t,u)$, t and u are time and the along-track positions, and k and k_u are their respective wavenumbers;

$$\mathrm{w}_p(k,k_u) = a_p\left[\mathrm{round}\left(\frac{k-k_0}{\Delta k}\right),\mathrm{round}\left(\frac{k_u-k_{u,0}}{\Delta k_u}\right)\right]$$

is a window function that implements the random block assignment over a grid with centres at the wavenumbers $(k_i,k_{u,j})=(k_0+i\Delta k_i,k_{u,0}+j\Delta k_{u,j})$, where $a_p[i,j]$ is a 2-D pseudo-random noise sequence drawn from a binary distribution, $\mathrm{round}(x)$ is the nearest integer to x, and the subscript p denotes the pth sequence realisation. The SAS images for a pair of complimentary looks $i_p(x,y)$ and $\bar{i}_p(x,y)$ can then be generated from the data, i.e.,

$$i_p(x,y) = \mathrm{IM}\{\mathrm{FT}^{-1}\{D_p(k_u,k)\}\}$$

$$\bar{i}_p(x,y) = \mathrm{IM}\{\mathrm{FT}^{-1}\{\overline{D}_p(k_u,k)\}\},$$

where $\mathrm{IM}\{\cdot\}:t,u\rightarrow x,y$ is the SAS imaging operator, and x and y are the along-track and across-track image coordinates.

Other schemes can also be conceived to obtain the multiple looks, including using vertically separated receivers or multiple passes.

2.2. Coherence of Wavelet Coefficients

The wavelet domain is good for yielding sparse image representations, meaning that the important information tends to be contained within only a few coefficients whereas noise is distributed more evenly. It is therefore, a good domain for separating targets from noise and has been used for resolution-preserving de-noising in imaging applications, including sonar [13].

The images for the complimentary looks can be transformed to the wavelet domain by the discrete wavelet transform, i.e.,

$$C_p(x',y',s) = \mathrm{WT}\{i_p(x,y)\}$$

$$\overline{C}_p(x',y',s) = \mathrm{WT}\{\overline{i}_p(x,y)\},$$

where the operator $\mathrm{WT}\{\cdot\}: x,y \to x',y',s$ denotes the wavelet transform and s is the wavelet scale. The transform is phase-preserving when symmetric / anti-symmetric wavelet pairs are used, and this is important for retaining the phase information in subsequent signal processing.

The coefficients corresponding to targets or noise are distinguished by considering a measure of their similarity between the looks; coefficients that are similar are designated as belonging to a potential target whereas those that are dissimilar are designated as noise. The similarity is quantified here using the coherence but other metrics can also be used [10,11]. The coherence between looks can be estimated using

$$\rho_p(x',y',s) = \frac{\sum_{m,n=-(N-1)/2}^{(N-1)/2} C_p(x'+m\Delta x, y'+n\Delta y, s)\overline{C}_p^*(x'+m\Delta x, y'+n\Delta y, s)}{\sqrt{\sum_{m,n=-(N-1)/2}^{(N-1)/2} \left|C_p(x'+m\Delta x, y'+n\Delta y, s)\right|^2}\sqrt{\sum_{m,n=-(N-1)/2}^{(N-1)/2} \left|\overline{C}_p^*(x'+m\Delta x, y'+n\Delta y, s)\right|^2}}$$

for an N×N averaging window, where Δx, Δy are the pixel dimensions. The variance of the coherence estimate can be reduced by averaging over a larger window (i.e., larger N) at the cost of reduced spatial resolution. The variance can also be reduced by averaging over a number P of different look realisations, i.e.,

$$\rho(x', y', s) \approx \frac{1}{P} \sum_{p=1}^{P} \rho_p(x', y', s),$$

where, for example, the different looks are obtained by repartitioning the data with different realisations of the pseudo-random noise sequence.

2.3. Shrinkage of Wavelet Coefficients

Having determined the coherence of the wavelet coefficients, a weighting scheme is chosen to attenuate those coefficients that are deemed to be incoherent and therefore designated as noise. The derivation of an optimal weighting scheme will depend on the assumed properties of the targets, background reverberation, and the system parameters; this is an interesting subject for future research. However, to demonstrate the principle we define here a simple ad-hoc scheme with a user-defined soft threshold, i.e., with weights

$$A(x', y', s) = \begin{cases} 1, & \rho(x', y', s) > \rho_{\max} \\ 0, & \rho(x', y', s) < \rho_{\min} \\ \dfrac{\rho(x', y', s) - \rho_{\min}}{\rho_{\max} - \rho_{\min}}, & \text{otherwise} \end{cases}$$

where coefficients with coherence less than $\rho_{\min}$ are attenuated completely and coefficients greater than $\rho_{\max}$ are retained completely, with a linear graduation between these thresholds.

(a)  (b) 

Figure 3 – MUD low frequency broadband synthetic aperture sonar: (a) wet-end; (b) deployment.

Using these coherence-based weights, the wavelet coefficients of the full image are adjusted and then inverse wavelet transformed to yield the image containing only the coherent targets, i.e.,

$$i'(x,y) = \mathrm{WT}^{-1}\{A(x',y',s)\,\mathrm{WT}\{i(x,y)\}\},$$

where

$$i(x,y) = \mathrm{IM}\{\mathrm{FT}^{-1}\{D(k_w,k)\}\}$$

is the full SAS image.

3. Results from the MUD Sonar

The MUD system is a low-frequency broadband synthetic aperture sonar developed by TNO for experimentation on buried object detection [3]. The system wet end is shown in Figure 3. It is comprised of an exchangeable acoustic projector, two 16-element hydrophone arrays, and navigation sensors (real-time kinematic GPS and a photonic INS). These components are

mounted on a frame with an adjustable tilt angle that is adapted for operation from diver support vessels of the Royal Netherlands Navy.

Using a 4-9 kHz projector and a sidescan imaging geometry, the system is capable of detecting objects completely buried in mud at ranges up to 70 m in very shallow water (approximately 10-15 m water depth and 0.5 m of mud). Figure 4(a) shows a SAS image acquired by the system during a 2011 sea trial in the Haringvliet [8]. A test garden consisting of a variety of different objects was deployed for the trial, including mine-like and non mine-like objects, unexploded ordinance (UXOs), and calibration targets. These objects were actively buried by divers 6 months prior to the trial. A high-frequency sonar survey was conducted immediately before the trial using a REMUS AUV and this confirmed that the objects were indeed buried (i.e., they were not detected during the REMUS survey). The contacts corresponding to the deployed objects were identified using ground-truth measurements and these are indicated by arrows in the SAS image of Figure 4(a). This demonstrates the capability of the system to detect the buried objects. However, in addition to the objects of interest, the system also detects regions of dense clutter, an example of which has been indicated within the boxed area of Figure 4(a). In some cases, the high clutter density prevents the confident matching of target contacts with the ground-truth. It is clear from this example that robust classification is required to discriminate between targets and clutter in order to achieve an operational capacity.

Isolation of the contact responses from the background reverberation is a crucial pre-processing step in the classification procedure. The proposed wavelet shrinkage technique is demonstrated here for this purpose. The technique was applied to the SAS image of Figure 4(a) using the following parameters: the data support in wavenumber space was partitioned into a grid

of 32×32 blocks to generate the complementary looks; a window of $N = 5$ pixels was used to estimate the coherence (image pixel size of $\Delta x = 0.2$ m and $\Delta y = 0.1$ m); the coherence was averaged over $P = 100$ look realisations; and a soft threshold of $\rho_{min} = 0.4$ and $\rho_{max} = 0.5$ was used to weight the wavelet coefficients. The separated contacts and background are shown in Figure 4(b) and (c), respectively. Qualitatively, it can be observed that the contacts have been well isolated and that the resolution has been preserved.

The procedure is shown in more detail in Figure Figure 5 for a specific target: the EVA cylinder [14] from NATO's Centre for Maritime Research and Experimentation (CMRE). A photograph of the EVA cylinder is shown in Figure 5(a). The cylinder is 1.5m long and 0.5m in diameter with hemispherical end-caps, it is constructed from a thin shell of composite material and filled with water except for one end-cap which is solid epoxy resin. Figure 5(b) shows the SAS image snippet. A single realisation of the randomly partitioned wavenumber space used to generate a look is shown in Figure 5(c), the wavelet transform of the look image is shown in Figure 5(d), and its coherence with respect to the complimentary look image is shown in Figure 5(e). The coherence of the wavelet coefficients between the complimentary looks is very noisy for a single realisation but this is reduced significantly by averaging the coherence over multiple complimentary look realisations, as shown in Figure 5(f).

The SAS image snippet for the isolated response of the EVA cylinder is shown in Fig 6(a). The corresponding echo data (obtained by reversal of the SAS imaging operator) are shown in Figure 6(c) and the multi-aspect acoustic colour (i.e., the aspect-frequency representation of the echo data) is shown in Figure 6(d). For comparison, Figure 6(b), (d), and (e) show respectively the SAS snippet, echo data, and multi-aspect acoustic colour, where the target isolation has been achieved by application of a window of dimensions 2.5 x 5 m with a 0.5 m transition border. In

this case, the window is too large and some of the background is retained, thus corrupting the target response. Conversely, when the window is too small important details can be lost.

3.1. Quantitative Analysis

The procedure was repeated for a variety of targets over different runs to gain a quantitative estimate of the average improvement offered by the method. The targets considered were: 1) the EVA cylinder, 2) a replica 155 mm shell (UXO), 3) a boulder of approximately 40 cm diameter, and 4) SESAME – a pressurised container containing underwater acoustic logging equipment. These targets are indicated in the SAS image of Figure 4 by the identifiers EVA, SHL2, BOU2, and SES, respectively. The improvement is quantified using an estimate of the signal-to-reverberation ratio (SRR) given by

$$\mathrm{SRR} = \max\left(|i(x,y)|^2\right) / \mathrm{median}\left(|i(x,y)|^2\right)$$

over an image snippet of dimensions 10 x 10 m centered on the target. The results are tabulated in Figure 7 and show an average SRR improvement between 15 and 20 dB.

4. Conclusion and Discussion

A wavelet shrinkage algorithm has been presented for the enhancement of the acoustic response of coherent targets in low frequency synthetic aperture sonar imagery. The algorithm has been demonstrated on data from the TNO MUD low frequency sonar and shown to suppress the background seafloor reverberation effectively, achieving an average increase in SRR of between 15 and 20 dB whilst preserving image resolution and phase. Further work is required to investigate the optimal generation of complimentary looks based on prior knowledge of the reverberation and target coherence and optimal thresholding schemes.

Acknowledgments

This work was partially funded by the US Department of Defense Strategic Environmental Research and Development Program (SERDP) and the authors thank Dr. Herb Nelson of SERDP for his support. The authors also acknowledge the Royal Netherlands Navy for funding and operational support for the MUD sea trials and the NATO Centre for Maritime Research and Experimentation (CMRE) for providing the EVA cylinder.

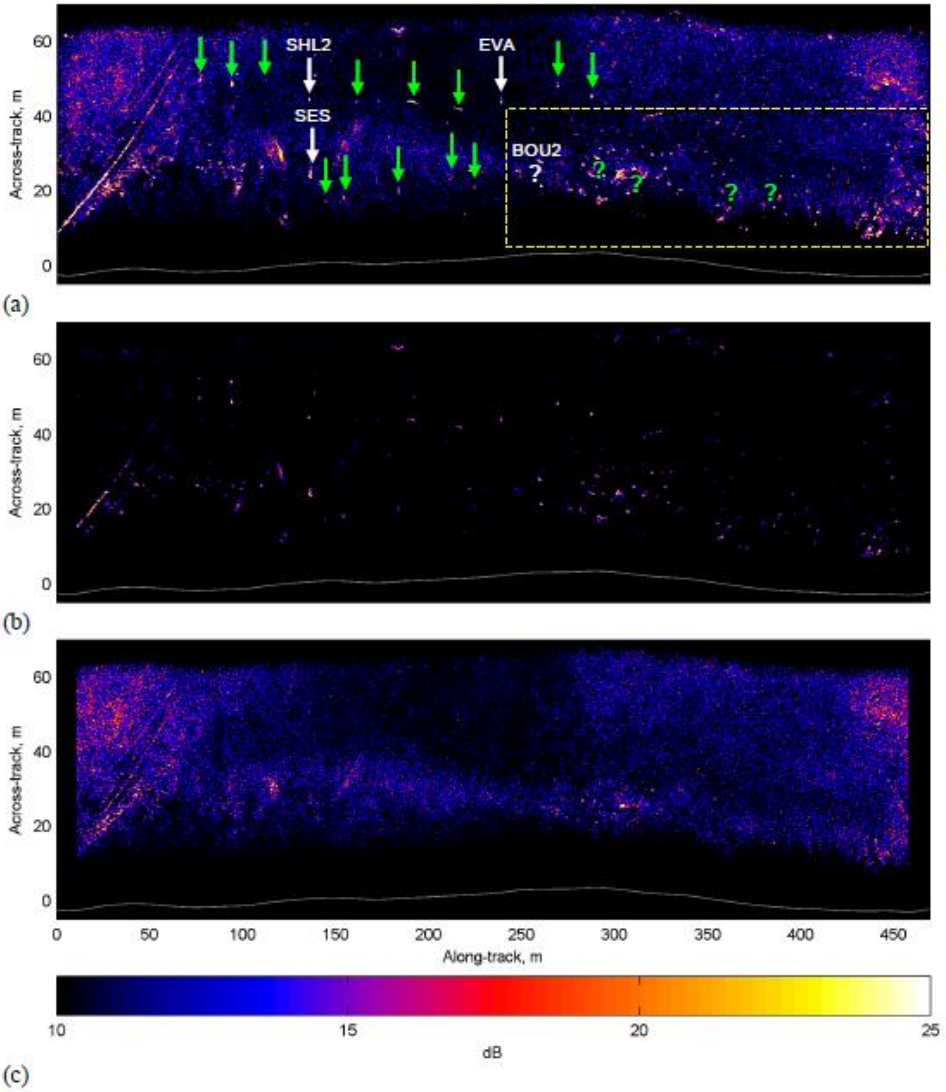

Figure 4 – Run 325 from the MUD-2011 trials: (a) SAS image with contacts of the deployed targets indicated by arrows and an area of dense clutter indicated within the yellow boxed region; for this run, the contacts corresponding to deployed objects could not be identified with confidence in this region and the ground truth locations are indicated by the question marks; (b) coherent contacts and (c) background noise separated using the wavelet shrinkage method.

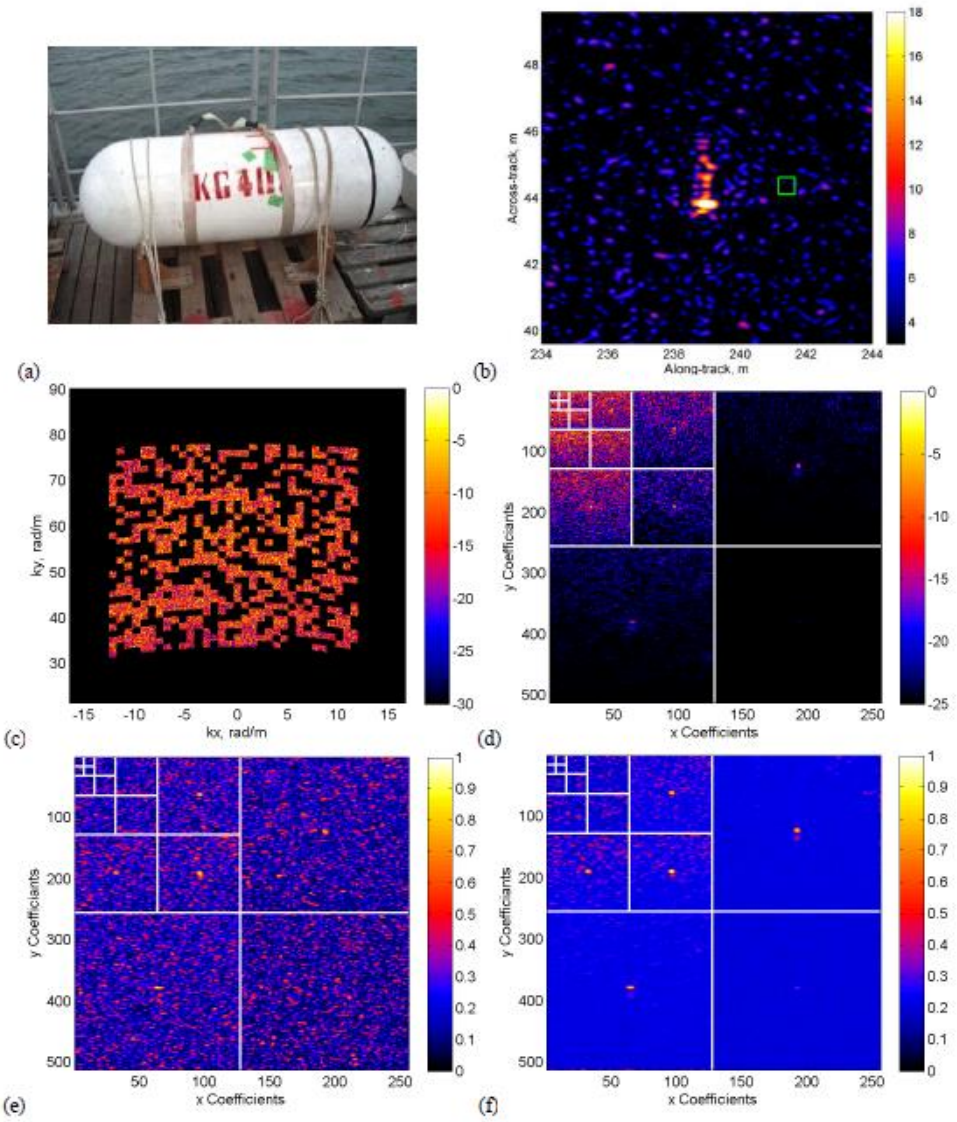

Figure 5 – Target / background separation for the CMRE EVA cylinder target: (a) photograph of the EVA cylinder; b) SAS image snippet (the green square denotes the ground-truth location); (c) wavenumber spectrum of a random look realisation; (d) wavelet decomposition of the look image; (e) wavelet coherence between a pair of complimentary looks; (f) average wavelet coherence over 100 look realizations.

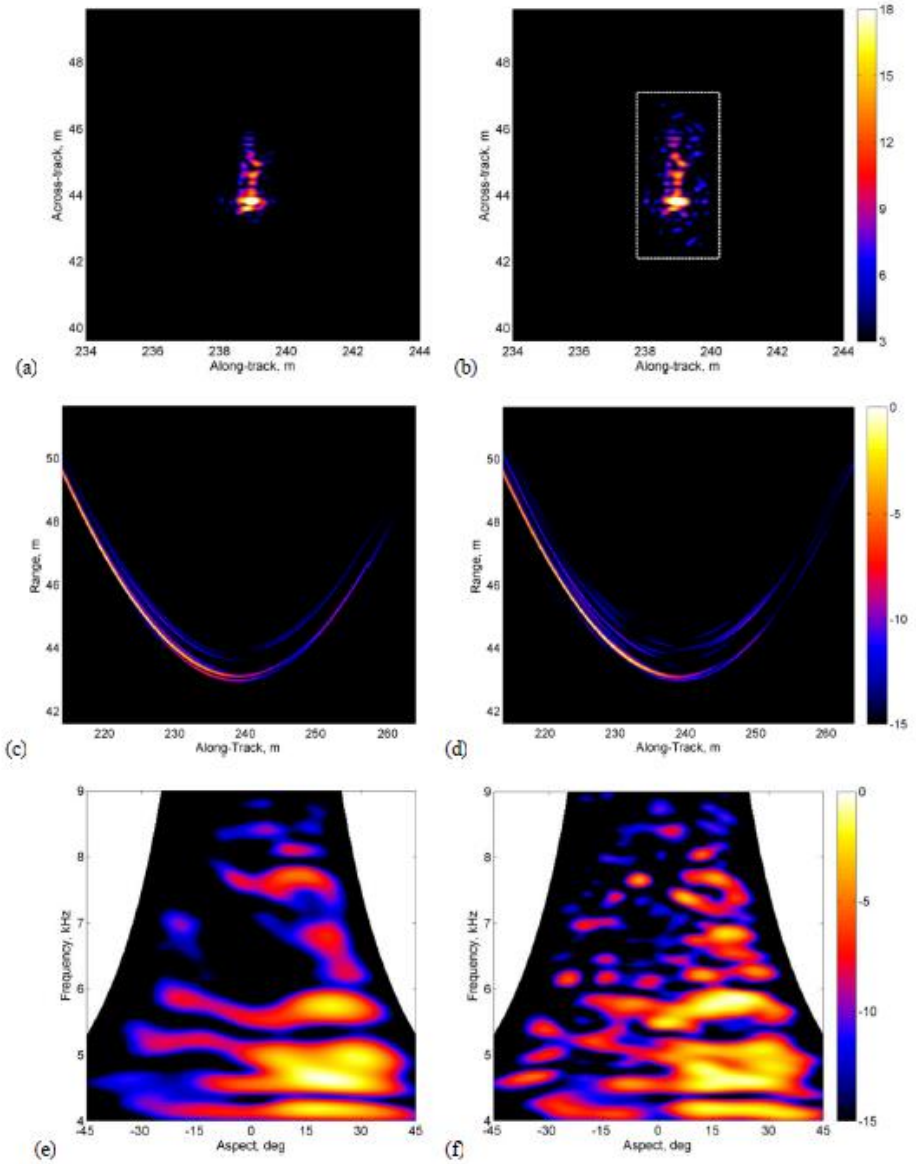

Figure 6 – Acoustic signatures of the EVA target obtained using: (a,c,e) the wavelet shrinkage method with a soft threshold for the coherence between 0.4 and 0.5; and (b,d,f) a spatial window of dimensions 2.5 x 5 m. (a,b) shows the SAS image snippet, (c,d) the echo data, and (e,f) the multi-aspect acoustic colour.

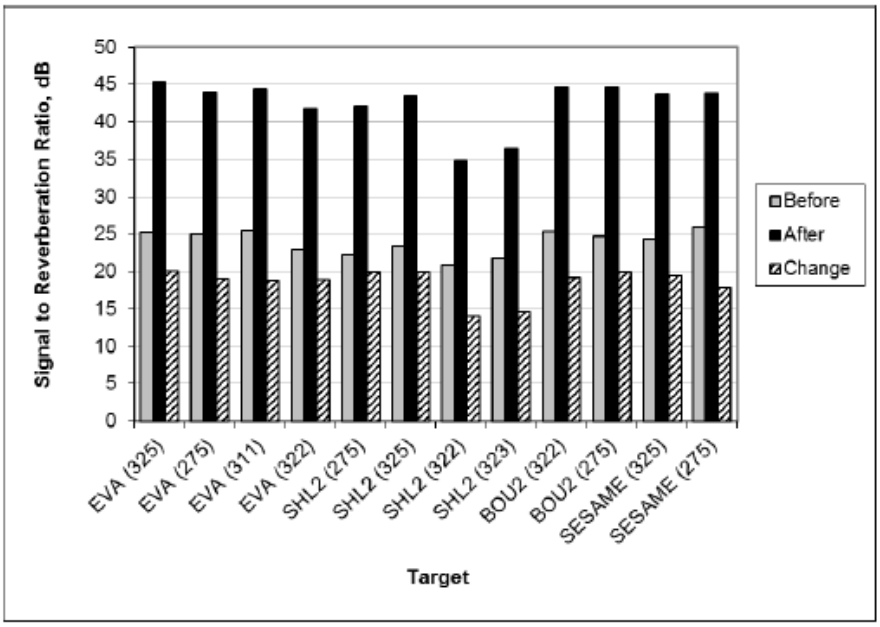

Figure 7 – Comparison of estimated signal-to-reverberation ratio before and after target enhancement by incoherent wavelet shrinkage.

References

[1] J. A. Bucaro *et al.*, "Broadband acoustic scattering measurements of underwater unexploded ordinance", J. Acoust. Soc. Am., vol. 123, no. 2, 2008

[2] K. L. Williams *et al.*, "Acoustic scattering from a solid aluminum cylinder in contact with a sand sediment: measurements, modeling, and interpretation" J. Acoust. Soc. Am., vol. 127, no. 6, 2010

[3] A. L. D. Beckers, R. van Vossen, and G. Vlaming, "Low-frequency synthetic aperture sonar for detecting explosives in harbours", Sea Technology Magazine, vol. 53, no. 3, 2012

[4] D. Sternlicht *et al.*, "Advanced sonar technologies for autonomous mine countermeasures", in Proc. Oceans, Hawaii, USA, 2011.

[5] S. G. Schock, J. Wulf, G. Quentin, and J. Sara, "Synthetic aperture processing of buried object scanning sonar data", in Proc. Oceans, Washington DC, USA, 2005.

[6]B. J. Davis, P. T. Gough, and B. R. Hunt, "Modeling surface multipath effects in synthetic aperture sonar", IEEE J. Ocean. Eng., vol. 34, no. 2, 2009

[7] M. Pinto, A. Bellettini, L.S. Wang, P. Munk, V. Myers, and L. Pautet, "A new synthetic aperture sonar design with multipath mitigation", in Proc. High Frequency Ocean Acoustics, American Institute of Physics, 2004.

[8] A. J. Hunter *et al.*, "Low frequency synthetic aperture sonar for detecting and classifying buried objects" in Proc. European Conference on Underwater Acoustics, 2012.

[9] P. Marston, T. Marston, and K. L. Williams, Scattering resonances, filtering with reversible SAS processing, and applications of quantitative ray theory", in Proc. MTS/IEEE Oceans, Sep 2010

[10] O. Tischenko, C. Hoeschen, and E. Buhr, "An artifact-free structure-saving noise reduciton using the correlation between two images for threshold determination in the wavelet domain", in Proc. SPIE Medical Imaging, 2005.

[11] R. A. Borsdorf, R. Raupach, T. Flohr, J. Hornegger, "Wavelet based noise reduction in CT images using correlation analysis", IEEE Trans. Med. Image, Vol. 27, No. 12, 2008

[12] J. W. Goodman, "Speckle phenomenon in optics: theory and applications", Roberts and Co. Publishers, 2006.

[13] C. K. Chui., "An introduction to wavelets", Academic Press, 1992.

[14] A. Tesei, "At-sea measurements of acoustic elastic scattering by a 1.5m long cylinder made of composite materials", In Proc. Underwater Acoustic Measurements, 2007.

Appendix B Proceeding Paper for UAC 2013, Corfu Greece

(Draft Version, to be submitted)

ACOUSTIC SIGNATURES OF UNDERWATER UXO MEASURED BY LOW FREQUENCY BROADBAND SAS

Alan Hunter[a], Robbert van Vossen[a] , Benoit Quesson[a], and Guus Beckers[a]

[a]TNO (Netherlands Organisation for Applied Scientific Research)

PO Box 96864, 2509 JG The Hague, The Netherlands, +31 88 866 0902,
alan.hunter@tno.nl

Abstract: The remediation of underwater unexploded ordnance (UXO) requires a capability to detect and classify objects bottom objects. This can be facilitated partly by use of modern high-frequency imaging sonar. However, this technology is limited in two respects: 1) the high frequencies employed by these systems cannot penetrate into the sediment to detect buried objects; and 2) the operational effectiveness and efficiency is severely limited by a high false alarm rate in cluttered environments. For these reasons, there is significant research efforts investigating the use of low frequency broadband sonar. In this paper, we demonstrate the latest experimental results from the MUD system. We show SAS images and multi-aspect acoustic colour plots of various objects (including UXO) buried beneath a layer of mud.

Keywords: Unexploded ordnance, low frequency, synthetic aperture sonar

1. INTRODUCTION

One of the most problematic areas where unexploded ordnance (UXO) can be situated is in an underwater environment, buried in sediment. Since burial frequently occurs in silt or mud, it is of great importance to have a capability for the detection of UXO in such buried conditions. We are investigating the detection of objects buried in mud using low frequency (LF) side-looking sonar. For this purpose, we have developed an experimental hull-mounted system referred to as the MUD system [1].

The detection of buried UXO with LF side-looking sonar is a challenging problem. This is primarily caused by high reverberation and possible clutter. In addition, the amplitude of the target echo of an object is reduced by burial. For these conditions,

dedicated processing has been developed to aid the detection of UXO and other targets of interest, and for the subsequent discrimination between targets and clutter contacts. This processing is outlined here, and results are presented for two buried targets: a 1.5m cylinder and a 155mm shell.

2. DATA PROCESSING CHAIN

2.1. Multipath Suppression

Multipath reverberation is problematic for low-frequency sonars with wide vertical beams operating in shallow water. Strong multipath interference can mask the echoes from targets and corrupt their acoustic signatures, adversely affecting detection and classification performance. This can be mitigated by using a vertical hydrophone array to steer the receive beam towards the seafloor and away from the sea surface.

For a regular linear array of M hydrophones with spacing Δz, the beam-steered echo data for a point of interest $\mathbf{x} = (x,y,z)$ on the seafloor is given by

$$d(u,t;\mathbf{x}) = \frac{c}{2\pi}\int_{-\infty}^{\infty} D(u,k;\mathbf{x})\exp(jkct)\,dk, \tag{1}$$

where u is the along-track distance, t is time, and c is the acoustic propagation speed;

$$D(u,k;\mathbf{x}) = \sum_{m=0}^{M-1} D_m(u,k)\exp(-j(k+k_0)(m-M/2)\Delta z\sin(\phi-\phi_0)) \tag{2}$$

is the summation of appropriately phase-adjusted echo spectra, where $k = 2\pi f / c$ is the wavenumber, f is frequency, and k_0 is the wavenumber at the basebanding frequency;

$$D_m(u,k) = \int_{-\infty}^{\infty} d_m(u,t)\exp(-jkct)\,dt \tag{3}$$

is the temporal spectrum of the basebanded echo data from the mth hydrophone (ordered from top to bottom), and

$$\phi(u,\mathbf{x}) = \sin^{-1}((z-z_s(u))/r(u,\mathbf{x})), \tag{4}$$

$$r(u,\mathbf{x}) = \sqrt{(x-x_s(u))^2+(y-y_s(u))^2+(z-z_s(u))^2} \tag{5}$$

are the declination angle and range from the sonar position $\mathbf{x}_s(u) = (x_s(u), y_s(u), z_s(u))$ to the point $\mathbf{x}$, and ϕ_0 is the tilt angle of the array (0 deg and 90 deg corresponding to side and down-looking geometries, respectively).

2.2. Synthetic Aperture Sonar (SAS) Imaging

Synthetic aperture sonar (SAS) uses coherent processing of the echo data to attain very high resolution in along-track. This is important for LF sonars, which typically have poor resolution due to their wide beams. The time-domain back-projection algorithm [2] is well-suited for this purpose since wide-beam motion compensation is easily accommodated compared with the faster Fourier-domain algorithms [3]. To accommodate a broad bandwidth, the procedure can be applied in sub-bands, as described below.

The broadband SAS image is obtained via a summation of back-projected images over N frequency sub-bands, i.e.,

$$i(x,y)=\sum_{n=0}^{N-1} i^{(n)}(x,y), \tag{6}$$

where the image for the nth sub-band is given by

$$i^{(n)}(x,y)=\int_{-\infty}^{\infty} w^{(n)}(u;\mathbf{x})\, d^{(n)}(u,2r(u,\mathbf{x})/c;\mathbf{x})\exp(jk_0 2r)du, \tag{7}$$

$r(u,\mathbf{x})$ is given by eq. (5), and

$$d^{(n)}(u,t;\mathbf{x})=\frac{c}{2\pi}\int_{f_{n,min}}^{f_{n,max}} D(u,k;\mathbf{x})\exp(jkct)\,dk \tag{8}$$

is the band-pass filtered echo data (after vertical beam-steering) for frequencies $f_{n,min}$ to $f_{n,max}$. The along-track integration limits for each sub-band are constrained to the opening angle of the horizontal beam at the sub-band upper frequency limit $f_{n,max}$ via the window function

$$w^{(n)}(u;\mathbf{x})=\begin{cases}1, & |\theta(u,\mathbf{x})|<\theta_0(f_{n,max})\\ 0, & \text{elsewhere}\end{cases}, \tag{9}$$

where

$$\theta(u,\mathbf{x})=\tan^{-1}((x-x_s(u))/(y-y_s(u))) \tag{10}$$

is the azimuth angle from the sonar position $\mathbf{x}_s(u)$ to the point $\mathbf{x}$, and $2\theta_0(f)$ is the (frequency-dependent) opening angle.

2.3. Fixed-Focus Enhancement of Resonances

In standard SAS imaging, each image pixel (x,y) is computed based on an assumed range-dependent locus of echoes $r(u,\mathbf{x})$, given by eq (5). However, this assumption is violated for resonant scattering since the resonant echoes originate at the spatial location of the object (corresponding to locus of a given curvature) but manifest in the data at longer ranges (with a locus of the same curvature). For a resonant object at a known location, it is therefore better to focus the resonant "tail" using a fixed focal point based on the location of the target $\mathbf{x}_F=(x,y_F,z)$ rather than the image pixel $\mathbf{x}$, i.e.,

$$r(u,\mathbf{x};\mathbf{x}_F)=\sqrt{(x-x_s(u))^2+y_F^2+(z-z_s(u))^2}-y_F+y \tag{11}$$

The same technique has been used previously for the enhancement of shadows [4].

2.4. Multi-Aspect Acoustic Colour Extraction via Reverse SAS

The multi-aspect acoustic colour (MAAC) is a representation of the sonar data that emphasises aspect and frequency dependencies and can yield possible features for target classification. A target's MAAC can be obtained from the SAS image by isolating the target from the background and other nearby scatterers, followed by a reversal of the SAS imaging process [3], i.e., the MAAC is given by

$$A(f,\theta)=D'(k,k\sin\theta), \tag{12}$$

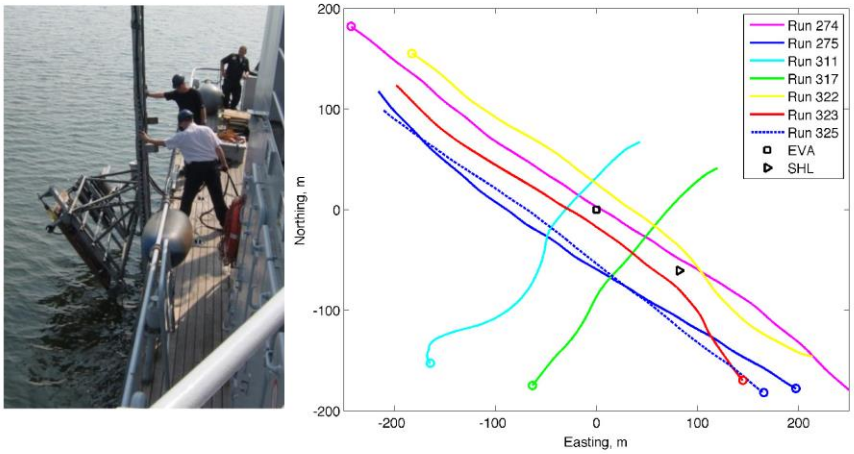

Figure 1 – (a) Deployment of the MUD system during the 2011 trial in Haringvliet, The Netherlands; (b) trajectories for a selection of runs and deployment ground-truth for the EVA cylinder and 155mm shell.

with respect to frequency f and azimuth angle θ, where

$$D'(k_u, k) = \int_{-\infty}^{\infty}\int_{-\infty}^{\infty} i'(x, y)\exp\left(-j\left[k_u x + \left(\sqrt{4(k + k_0)^2 - k_u^2} - 2k_0\right)y\right]\right)dx\,dy \qquad (13)$$

is the 2-D Fourier spectrum of the target echo data, which is obtained here via an inversion of the Stolt mapping on the SAS image of the isolated target $i'(x, y)$. The target can be isolated in the SAS image by simple windowing [3] or by a more sophisticated technique based on the shrinkage of incoherent wavelet coefficients [5].

3. RESULTS

3.1. MUD Sonar and 2011 Sea Trial

TNO have developed a LF broadband (1 kHz – 26 kHz) side-looking sonar for experimentation on buried object detection and, with funding and support from the Dutch Ministry of Defence (Figure 1), have conducted sea trials in relevant operational environments and conditions. The system has both a horizontal and vertical array to enable the suppression of multi-path propagation in shallow water and to support synthetic aperture sonar (SAS) processing. Experimental results from the MUD-2009 and MUD-2011 sea trials demonstrate that signatures corresponding to objects buried in mud can be observed in data acquired by the MUD system [1][3]. In the following section, we show results from the 4 kHz – 9 kHz frequency band.

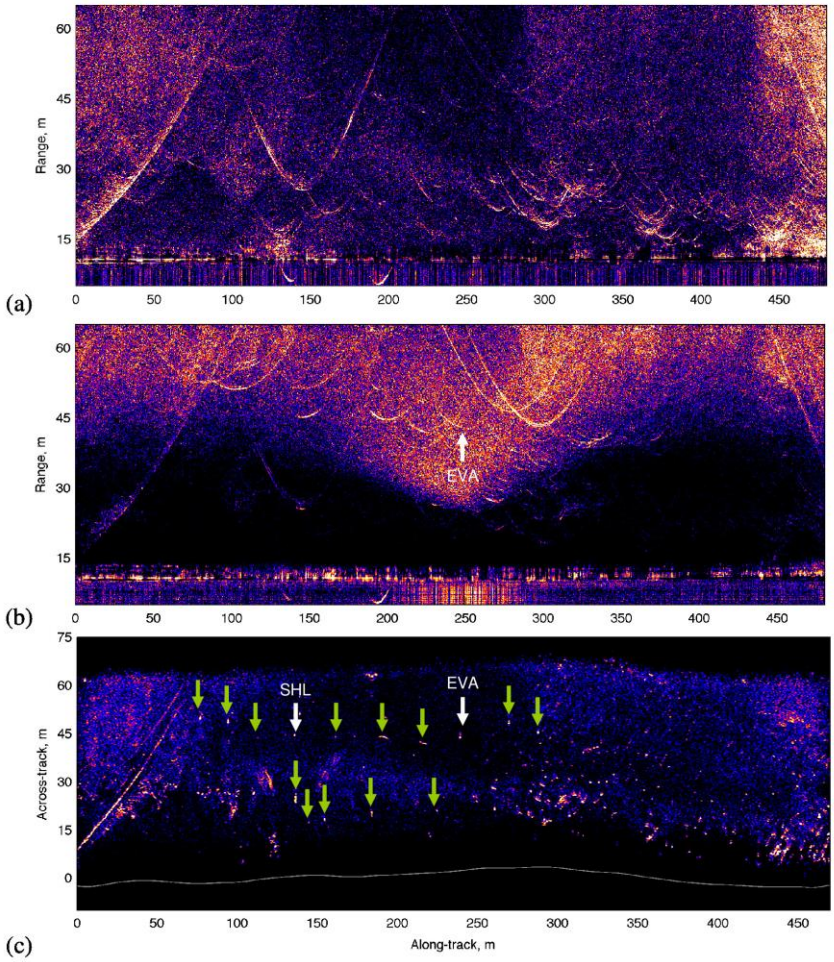

Figure 2 – Run 325: echo data from (a) a single hydrophone; (b) vertical array steered to the location of the EVA target; and (c) SAS image indicating the sonar path and the locations of the deployed targets.

3.1. SAS Images and Multi-Aspect Acoustic Colour

Results of the processing chain are illustrated in Figure 2 for an example run from the 2011 trial (run 325). The echo data corresponding to a single hydrophone clearly shows hyperbolas that correspond both to targets and seabed structures. One can also observe that most of these hyperbolas are only clearly visible up to a range of 30 m. At longer ranges, the signal-to-reverberation ratio (SRR) is reduced by multi-path propagation.

To mitigate the multipath contribution, vertical array beam-steering is used (Section 2.1). Figure 2b shows the effect of beam-steering to a single image position – the location of the EVA target. This procedure enhances the signal and reverberation directly received

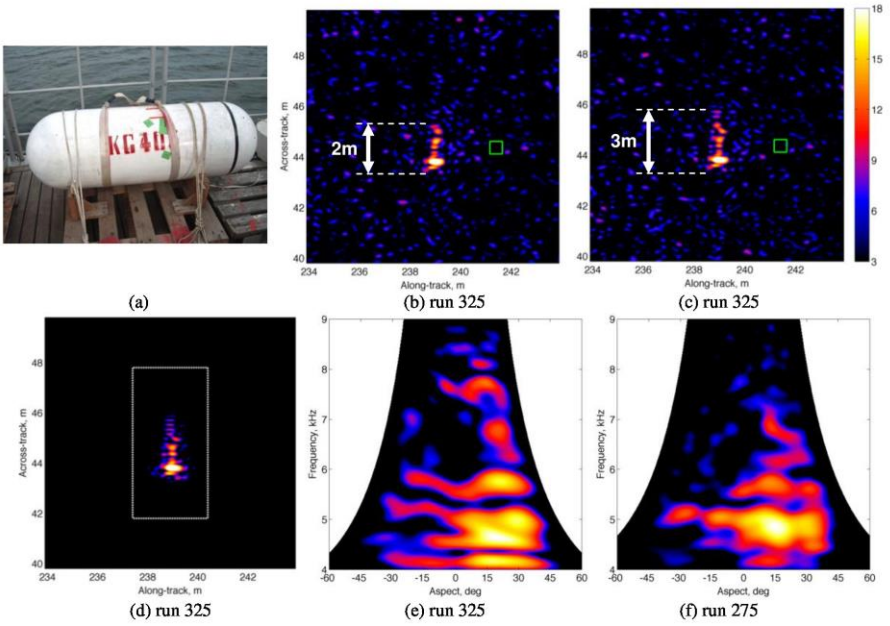

Figure 3 – (a) EVA cylinder; (b) SAS image for run 325 (the green square denotes the deployment ground-truth); (c) fixed focus SAS image, illustrating enhancement of the resonant tail; (d) target response after background suppression via wavelet shrinkage; (e) MAAC for run 325; (f) MAAC for run 275.

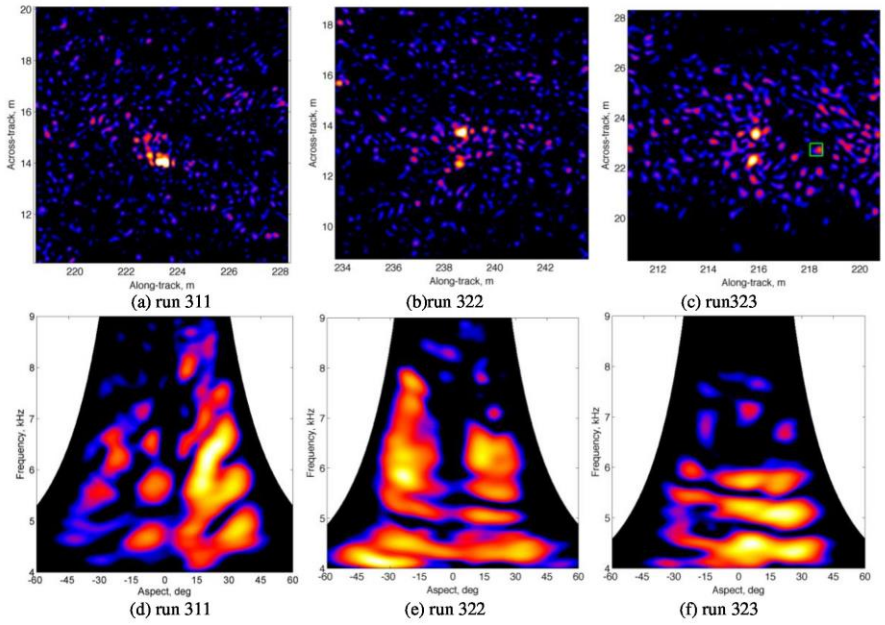

Figure 4 – EVA cylinder: SAS image and MAAC for runs (a,d) 311, (b,e) 322, and (c,f) 323.

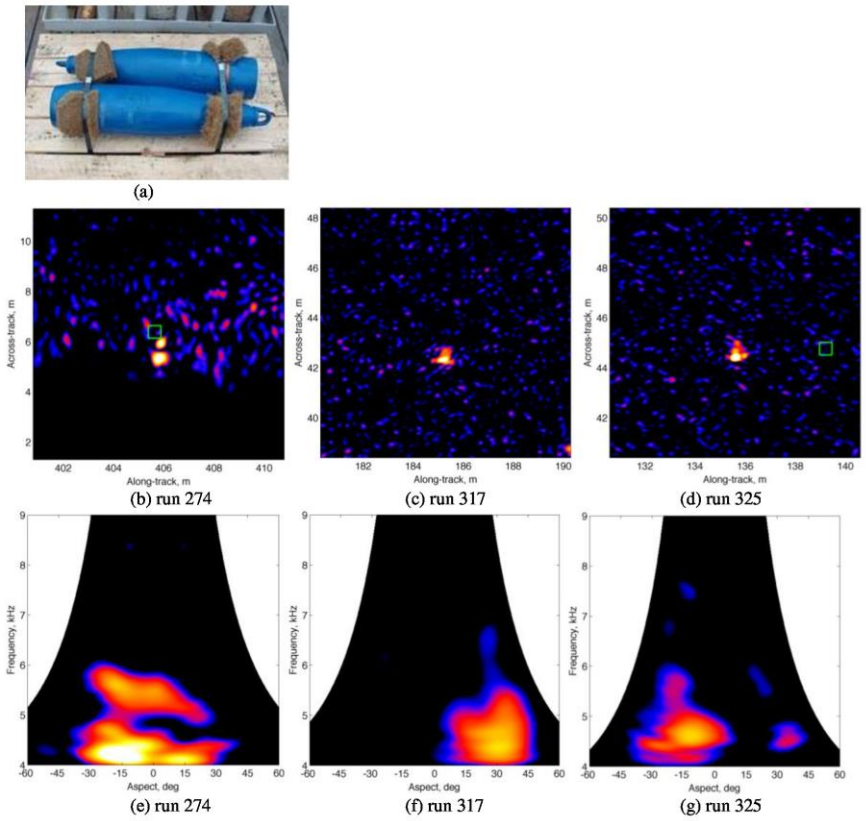

Figure 5 – 155mm shell: (a) photograph; SAS image and multi-aspect acoustic colour for runs (b,e) 274, (c,f) 317, and (d,g) 325.

from the seabed in this area, and mitigates the multipath. This vertical-array beam-steering is applied for all image positions, followed by the SAS processing (Section 2.2).

The resulting SAS image is shown in Figure 2c. Contacts corresponding to all the deployed targets can be observed. Most of these targets where buried, with a burial depth up to 0.50 m.

Figure 2c also shows a significant amount of clutter contacts originating from seabed structures and other unknown buried objects. Additional information is needed to distinguish man-made objects from these clutter contacts. In the remainder of this paper, we focus on the acoustic signatures of two targets: the EVA cylinder and a 155mm shell.

We start with the EVA cylinder. Fixed focus SAS processing (Section 2.3) is compared to conventional SAS processing in Figures 3b and 3c. It can be observed that the fixed-focus SAS processing results in a target signature with a longer tail in comparison to the conventional SAS processing. Fixed-focus SAS preserves resonances, whereas these are de-focused in conventional SAS. Because resonances are a potential classification feature for man-made objects, it is considered to be important to preserve these.

Figure 3d shows the result of enhancing coherent responses with respect to incoherent reverberation by using the wavelet shrinkage technique [5]. Multi-aspect acoustic colour (MAAC) signatures (Section 2.4) for two runs with similar trajectories are shown in

Figures 3e and f. One can observe similar patterns in these MAAC images, illustrating the repeatability. Figure 4 shows additional SAS and corresponding MAAC images of the EVA cylinder from different aspects (c.f., Figure 1). Repeatability is further supported by the results for runs 322 and 323 (Figure 4e and f). A clear difference can be observed with the MAAC response derived from run 311 (Figure 4d), which is perpendicular to the other runs. This is expected for cylindrical targets, since broadside target signatures substantially differ from end-on responses. We anticipate that this information can be used to aid the detection and classification.

Three results for a 155 mm shell are shown in Figure 5. SAS and MAAC images are shown for both short and long ranges at different angles. At this stage, it is difficult to interpret the results. An important difference with the EVA cylinder results is that only a response is obtained for frequencies below 6 kHz. It is unclear whether this is related to increased absorption due to larger burial depth of the 155 mm shell, or to characteristic target strength features of the shell. To aid the interpretation, we plan to compare the results to finite-element target echo modelling results for UXO targets [6].

4. SUMMARY

Dedicated processing has been developed to extract target acoustic signatures from data acquired by a low-frequency side-looking sonar system. It has been demonstrated that this processing enhances the signal-to-reverberation ratio and preserves resonances. Both are considered to be critical steps towards developing a detector for UXO buried in seabed sediments, since a capability is required to distinguish these contacts from clutter.

5. ACKNOWLEDGEMENTS

This work was funded by the Department of Defense Strategic Environmental Research and Development Program (SERDP) and the authors thank Dr. Herb Nelson of SERDP for his support. The authors also acknowledge the Royal Netherlands Navy for funding and operational support for the MUD sea trials and the NATO Undersea Research Centre for providing the EVA cylinder.

REFERENCES

[1] **A.L.D. Beckers et al.**, Low-frequency synthetic aperture sonar for detecting explosives in harbors, Sea Technology Magazine pp. 15-18, March, 2012.

[2] **R.E. Hansen**, Introduction to synthetic aperture sonar, Sonar Systems, InTech, 2011.

[3] **A.J. Hunter et al.**, Low frequency synthetic aperture sonar for detection and classification of buried objects, 11th ECUA, Edinburgh, UK, 2012.

[4] **J. Groen et al.**, Shadow enhancement in synthetic aperture sonar using fixed focusing, IEEE Journal of Oceanic Engineering, 2009.

[5] **A.J. Hunter and R. van Vossen**, Enhancement of the low frequency broadband target response using SAS image coherence, 1st UAC, Corfu, Greece, 2013.

[6] **M. Zampolli et al.**, Low- to mid-frequency scattering from elastic objects on a sand sea floor: simulation of frequency and aspect dependent structural echoes, Journal of Computational Acoustics, 2012.

Appendix C Paper in Proceedings of ECUA 2012, Edinburgh, UK

Proceedings of the 11th European Conference on Underwater Acoustics

LOW FREQUENCY SYNTHETIC APERTURE SONAR FOR DETECTING AND CLASSIFYING BURIED OBJECTS

A.J. Hunter
R. van Vossen
B.A.J. Quesson
M.E.G.D. Colin
M. Zampolli
A.L.D. Beckers

TNO (Netherlands Organisation for Applied Scientific Research)
P.O. Box 96864
2509 JG The Hague
The Netherlands

1 INTRODUCTION

Sidescan high-frequency (HF) sonar (i.e., with frequencies higher than 100 kHz) is ideally suited for providing high-resolution images of the seafloor. However, since sound does not penetrate into the sediment at these frequencies, such systems cannot be used for the detection of buried objects, such as naval mines, improvised explosive devices (IEDs), and unexploded ordinance (UXO). Sidescan low-frequency (LF) sonar is a promising technology for the detection of objects buried in soft seafloor sediment. Acoustic energy is attenuated less by the sediment at lower frequencies and can therefore penetrate deeper, facilitating the detection of buried objects. Furthermore, a side-looking configuration yields a much higher area coverage rate compared to downward-looking systems (e.g., the BOSS system [1]), thus enabling efficient surveys.

In practice there are two fundamental issues with sidescan LF sonar. The resolution of conventional sidescan sonar is poor at low frequencies due to the lower directivity of the beams. Moreover, in addition to the targets of interest, many clutter contacts are also observed, including other buried objects (e.g., boulders) and geological features below the mud (e.g., sand ripples). Thus, a means of classification is necessary to distinguish between targets and clutter and to suppress the false alarms. Synthetic aperture sonar (SAS) processing is essential for attaining adequate image resolution and for facilitating object classification in order to realise an operational capacity.

The LF and HF classification problems are fundamentally different. While information on size and shape derived from high-resolution images are commonly used for HF classification, these are not reliable for LF classification since the wavelength is on the same order of magnitude as the dimensions of the objects of interest. However, structural resonances are generated in the objects at these frequencies and it is possible to exploit this. It has been indicated in experiments in controlled conditions and by modelling conducted by APL, NSWC-PC, and NRL, that useful information on the objects can be retrieved from the structural resonant features [2,3].

We are investigating data processing techniques for optimally extracting the multi-aspect acoustic colour (i.e., the aspect and frequency-dependent scattering characteristics) of objects from LF SAS data for the future purposes of detection and classification. In this paper, we describe the techniques, and present results from experimental data collected in operationally relevant environments and conditions.

2 MUD SYSTEM

The demonstrator system (referred to as the MUD system) is an LF SAS developed by TNO for experimentation on buried object detection. It has been used in several sea trials conducted with funding and support from the Dutch Ministry of Defence.

The system wet end is shown in Figure 1. It is comprised of an (exchangeable) acoustic source and two receiver arrays. Each array has 16 hydrophones; one array is orientated vertically and the other

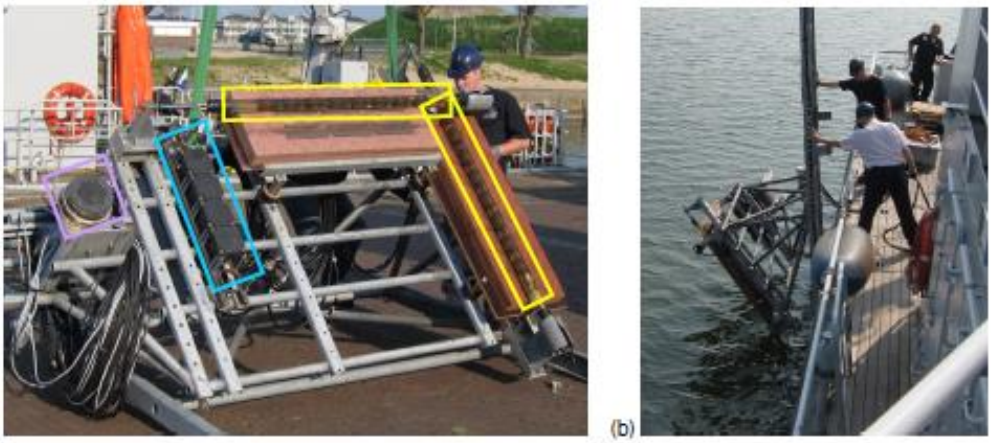

Figure 1 – MUD system (a) wet end, including receiver arrays (yellow boxes), LF source (blue box), and HF source (violet box); and (b) deployment.

Figure 2 – Location of the MUD-2011 sea trail: Haringvliet, The Netherlands (satellite image from Bing Maps).

horizontally. Three sources were available for the experiments, covering the bandwidths from 1 – 4 kHz (VLF), 4 – 9 kHz (LF), and 11 – 26 kHz (HF). The components are mounted on a frame with an adjustable tilt angle that is adapted for operation from diver support vessels of the Royal Netherlands Navy. Two navigation sensors are used to monitor the position and orientation of the sonar system; these are located on top of the support frame. A photonic inertial navigation system (PHINS) records the 3-D accelerations and rotation angles of the system and a real time kinematic global positioning system (RTK GPS) provides centimetre positioning accuracy. These non acoustical systems are necessary in order to derive the exact position and orientation of the system with respect to the test garden and also to assist with more advanced signal processing, in particular for the SAS processing.

Experimental results from the MUD-2011 sea trial in Haringvliet (shown in Figure 2) demonstrate that objects buried in mud can be detected in data acquired by the MUD LF SAS system [4].

3 DATA PROCESSING

3.1 Synthetic Aperture Imaging

Synthetic aperture sonar (SAS) uses coherent processing of the sidescan echo data to enhance the image resolution and the signal-to-reverberation ratio. SAS is essential for systems with wide beams (e.g., at low frequencies) since the conventional sidescan approach yields very poor resolution.

A SAS image $i(r, x)$ can be generated efficiently from the baseband echo data $d(t, u)$ via the inverse Stolt mapping in the Fourier domain (the wavenumber algorithm) [5], i.e.,

$$I(k_r, k_x) = D\left(\frac{1}{2}\sqrt{k_x^2 + (k_r + 2k_0)^2} - k_0,\ k_x\right),$$

where

$$D(k, k_u) = \int_{-\infty}^{\infty}\int_{-\infty}^{\infty} d(t,u)\exp(-j[kct + k_u u])\,dt\,du$$

$$I(k_r, k_x) = \int_{-\infty}^{\infty}\int_{-\infty}^{\infty} i(r,x)\exp(-j[k_r r + k_x x])\,dr\,dx$$

are the Fourier transforms of the echo data and SAS image, respectively; (r, x) are the slant-range and along-track image coordinates, (k_r, k_x) are the image wavenumbers, u is the along-track position of the sonar, t is time, (k, k_u) are the data wavenumbers, $k_0 = 2\pi f_0 / c$ is the wavenumber at the centre frequency f_0, and $c \approx 1500$ m/s is the propagation speed. The process is also reversible allowing the echo data to be recovered from the SAS image via the forward Stolt mapping, i.e.,

$$D(k, k_u) = I\left(\sqrt{4(k + k_0)^2 - k_u^2} - 2k_0,\ k_u\right).$$

In practice, the implementation details are subtle and care must be taken to ensure adequate sampling of the synthetic array and to minimise interpolation errors.

3.2 Wide Beam Sway Compensation

In an operational environment, the sonar does not follow a perfectly straight path as assumed above. Uncompensated deviations from a straight path introduce defocusing in the form of blurring and the introduction of artefacts; uncompensated sway (motion in the y direction) is the most problematic. Sway compensation is more complicated for systems with wide horizontal beams than it is for narrow beam systems [6]. However, an approximation can be made for small sub-images by performing the compensation relative to the sub-image centre.

The approximate wide beam sway compensation for a sub-image centred at the ground position $\mathbf{x}' = (x', y', z')$ is given by

$$d'(t, u \mid \mathbf{x}') = \int_{-\infty}^{\infty}\left[\int_{-\infty}^{\infty} d(t,u)\exp(-jkct)\,dt\right]\exp(j[(k + k_0)\,2\,\Delta r(u \mid \mathbf{x}') + kct])\,dk,$$

where

$$\Delta r(u \mid \mathbf{x}') = \sqrt{(x'-u)^2 + (y'-Y(u))^2 + (z'-Z)^2} - \sqrt{(x'-u)^2 + y'^2 + (z'-Z)^2}$$

is the range error relative to the subimage centre for the actual path positions $(u, Y(u), Z)$ with respect to the assumed straight path positions $(u, 0, Z)$, $Y(u)$ is the sway and Z is the sonar depth. In principle, the full image can be compensated by tiling many compensated subimages.

3.3 Vertical Array Processing

Multipath reverberation is a problem for sonar systems with wide vertical beams operating in shallow waters. Strong multipath interference due to the shallow water waveguide causes a reduction in image contrast and corruption of the phase responses from the targets and the seafloor; this degrades detection and classification capabilities. The receiver-side multipath interference can be mitigated by use of a vertical receiver array to narrow the vertical beam and steer it towards the seafloor. For a vertical array of N hydrophones with a vertical spacing of Δz, and assuming a flat seafloor of depth z', the beamsteered image is given by

$$I(k_r, k_x \mid y) = \sum_{n=-N/2}^{N/2-1} I_n(k_r, k_x) \exp\left(j \frac{1}{2} \sqrt{k_x^2 + (k_r + 2k_0)^2}\; n \Delta z \sin\phi(y) \right),$$

where $I_n(k_y, k_z)$ is the Fourier-domain SAS image from the nth hydrophone,

$$\phi(y) = \tan^{-1}\left(z' / \sqrt{y^2 - z'^2} \right) - \phi_0$$

is the steering angle for the across-track position $(\cdot, y, z')$ and ϕ_0 is the tilt angle of the array. A vertical array can also be used as an interferometer to infer the target heights and seafloor bathymetry.

At very low frequencies (e.g., less than 2 or 3 kHz), the array size required to achieve an adequately narrow beam starts to become impractical due to the long wavelengths (e.g., $\lambda = 0.5$ m at $f = 3$ kHz). Furthermore, higher order multipath modes remain a problem since the angles of arrival can be very close to the angle of the direct arrival from the seafloor, particularly at longer ranges [7].

3.4 Multi-Aspect Acoustic Colour

The multi-aspect acoustic colour is a representation of the sonar data that emphasizes aspect and frequency-dependent scattering characteristics. It is possible to extract the acoustic colour of a specific object using a windowed SAS image snippet; the object's response must be well resolved from the responses of any other nearby objects and with minimal influence from the surrounding seafloor and multipath reverberation. This information can be potentially exploited for classification purposes. It is especially relevant at low frequencies, where high-frequency classification methods based on characterisation of the size and shape of an object's echo and shadow are unreliable and where the frequencies cover a range for which interesting target resonances can occur.

The multi-aspect acoustic colour is obtained from the SAS image snippet via a remapping $k_u = k \sin\theta$ of the Fourier domain data, i.e.,

$$A(f, \theta) = D_{\text{win}}(k, k \sin\theta),$$

where $f = ck / 2\pi$ is the frequency, θ is the aspect to the object in the slant-range plane relative to the sonar path, and

$$D_{\text{win}}(k, k_u) = \int_{-\infty}^{\infty} \int_{-\infty}^{\infty} i(r, x)\, \text{win}(r, x) \exp\left(-j \left[\left(\sqrt{4(k + k_0)^2 - k_u^2} - 2k_0 \right) r + k_u x \right] \right) dr\, dx\,.$$

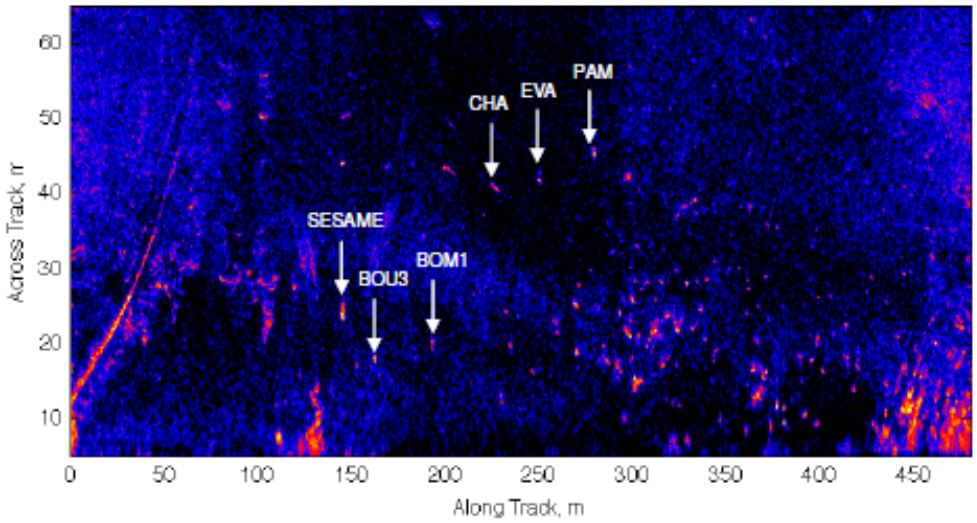

Figure 3 – SAS image of run 325 from the MUD-2011 sea trial. The image has a 15 dB dynamic range relative to the average seafloor reverberation level and sway compensation has not been applied.

is the Fourier domain data corresponding to the SAS image snippet $i(r,x)\mathrm{win}(r,x)$ and win is a window function that optimally isolates the response of the object from other nearby objects and the reverberation.

SAS processing, motion compensation, and multipath suppression, are all essential steps for allowing good isolation of the objects in the imagery for multi-aspect acoustic colour extraction.

4 EXPERIMENTAL RESULTS

Data has been collected using the MUD system during several sea trials, including the MUD-2011 trial [4] conducted in Haringvliet, an estuary in the Netherlands. The water depth in the test area is approximately 10 – 15 m and the seafloor has a sand bottom with a mud covering of thickness varying between approximately 40 cm and 130 cm. A test garden was deployed 6 months prior to the trial and the objects were actively buried by divers. The test garden is populated with a variety of different targets, including mine-like and non mine-like objects, UXOs, and calibration targets. The objects were distributed over three lines with an average distance between targets of approximately 25 m. The trial took place from 18 to 22 April 2011 and a total of 220 runs were executed covering different areas of the test garden. Control runs were also conducted using a REMUS AUV with a VHF (900 kHz / 1800 kHz) sidescan sonar immediately after deployment of the garden in February 2011 and during the trial in April 2011.

A portion of the dataset has been selected and processed to demonstrate the data processing steps described in Section 3. The selected data are from three runs using the LF (4 kHz – 9 kHz) acoustic source and covering the same area of the test garden. From bathymetric maps, the water depth in the area is known to be approximately 10 m to the mud surface. Each run covers a swath of 70 m over an along-track distance of 500 m and the ship travelled at an average speed of 1.8 m/s (3.5 knots) on a nominally straight course. Runs 275 and 325 follow the same track and run 322 follows a track on the opposite side of the swath.

The LF SAS image of run 325 is shown in Figure 3. The 16-element vertical receiver array was used to steer a beam toward the seafloor and sway compensation was not applied. Many focused

contacts can be observed. However, multipath replicas are observed behind some of the strong reflectors located at longer ranges. Aliasing artefacts due to undersampling of the synthetic array can also be observed; this is particularly evident for the strong scattering from the deployed SESAME target (an underwater acoustic logging system). In addition to the deployed targets within the footprint (all of which were observed), there are many unidentified clutter contacts; these are thought to be other objects and / or seafloor features. Based on the large number of clutter contacts, it is clear that dealing with false alarms is a very relevant operational issue.

The contacts associated with the deployed targets were identified in the SAS images using the GPS navigation data together with the known ground-truth for the deployment locations. An analysis of a selection of targets is shown in Figure 4 for a 10 m chain, a glass calibration sphere (PAM), 500 lb bomb (BOM1), and a 40 cm diameter boulder (BOU3) and in Figure 5 for the NURC EVA cylinder [8]. The chain, boulder, and EVA cylinder were not observed in the VHF imagery from the REMUS survey [4], indicating that these targets were completely buried in the mud. Sway compensation was applied to each SAS image snippet using sway estimates from the GPS data and the multi-aspect acoustic colour was extracted using 3 m x 3 m windows (a bigger 6 m x 3 m window was used for the chain). For the EVA cylinder, analyses from two different runs following the same track are presented to demonstrate that the results are repeatable. Note that the SAS images and acoustic colour plots exhibit speckle noise. The speckle has been reduced in the SAS images by averaging over wavenumber subbands; it can be reduced in the acoustic colour plots by averaging over multiple runs.

Based on the SAS image snippets alone, it is difficult to identify features that could be used to distinguish between the different objects reliably. However, it is apparent that the multi-aspect acoustic colour plots do exhibit some pronounced differences and a number of observations can be made. The EVA cylinder has a dominant response between 15 deg and 45 deg, suggesting that the axis of symmetry is orientated at approximately 30 deg relative to the track. Furthermore, it shows a strong modal response over the bandwidth, which seems to be consistent with the structural resonances for an *end-fire* orientation [8]. The chain has a very narrow angular response at approximately 15 deg, which is consistent with its long extent and observed orientation in the image. The calibration sphere and boulder both have omnidirectional responses. However, the boulder has a flat response whereas the sphere exhibits some modality. The bomb has a comparatively lower frequency response and appears to be orientated at approximately -10 deg relative to the track. A possible angular asymmetry can be observed, suggesting that the bomb may be orientated in a *broadside* geometry.

5 CONCLUSIONS

The detection of objects buried in mud has been demonstrated in an operational environment using a low-frequency sidescan synthetic aperture sonar. However, many unidentified clutter contacts were also observed in the SAS imagery. Classification of the contacts for distinguishing between targets and clutter is therefore of critical importance. Extraction of multi-aspect acoustic colour from the SAS image snippets of various different objects has been demonstrated in the LF band from 4 kHz to 9 kHz. The acoustic colours of various different objects have been shown to exhibit different characteristics. Furthermore, the acoustic colour extraction has been shown to be repeatable over different runs. These results give reason to believe that robust classification based on multi-aspect acoustic colour is possible.

Future work will focus on building a gallery of target signatures (SAS image snippets and multi-aspect acoustic colour plots) for various objects and clutter in the MUD sea trial data. Using the gallery, we hope to identify strategies for using the derived information for classification and false alarm reduction.

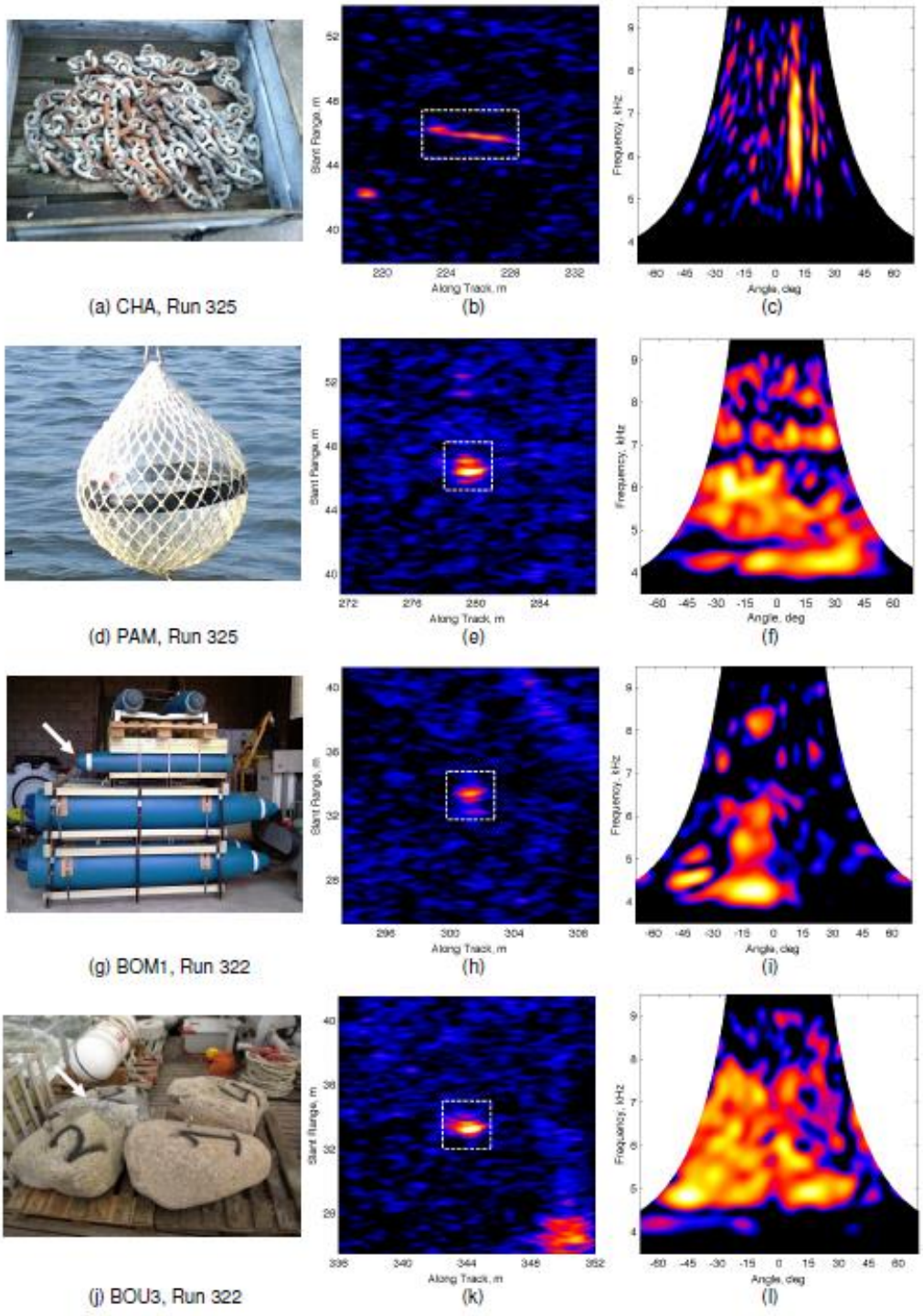

Figure 4 – Photographs (left column), SAS image snippets (middle column), and multi-aspect acoustic colour (right column) for a selection of targets. The dynamic range of the SAS images and acoustic colours is 15 dB.

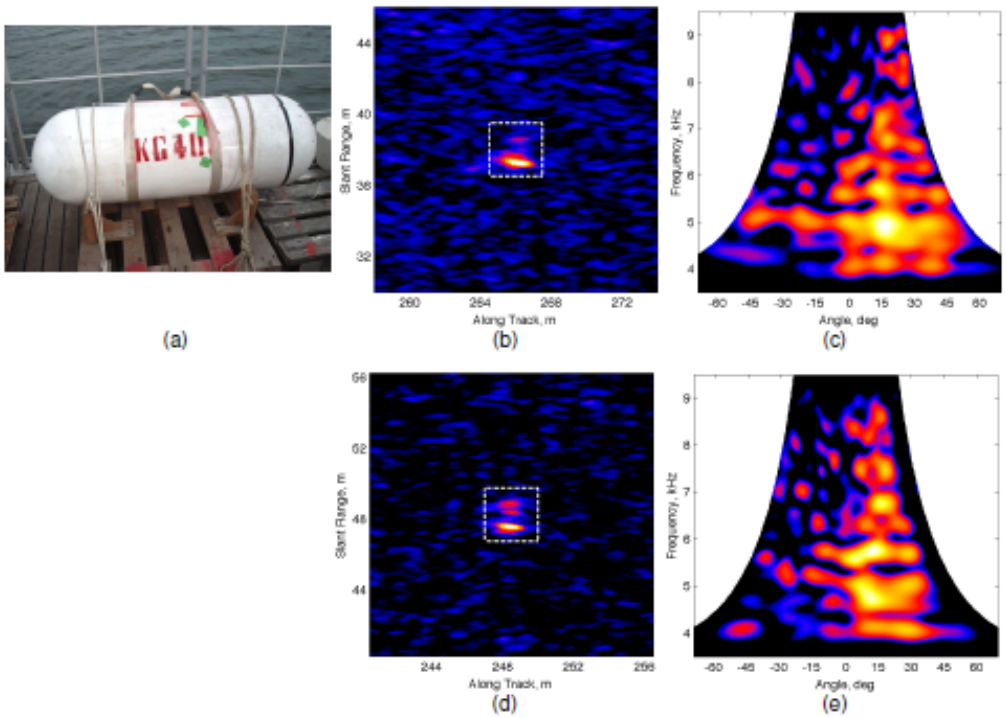

Figure 5 – EVA cylinder from two different runs with the same geometry: (b,c) run 275 and (d,e) run 325.

ACKNOWLEDGEMENTS

This work was funded by the Department of Defense Strategic Environmental Research and Development Program (SERDP) and the authors thank Dr. Herb Nelson of SERDP for his support. The authors also acknowledge the Royal Netherlands Navy for funding and operational support for the MUD sea trials and the NATO Undersea Research Centre for providing the EVA cylinder.

REFERENCES

1. D. Sternlicht *et al.*, Advanced sonar technologies for autonomous mine countermeasures, Proc. MTS/IEEE OCEANS. Hawaii, USA (Sep 2011).
2. J.A. Bucaro *et al.*, Broadband acoustic scattering measurements of underwater unexploded ordnance, Journal of the Acoustical Society of America, vol. 123, no. 2, 2008
3. K.L. Williams *et al.*, Acoustic scattering from a solid aluminum cylinder in contact with a sand sediment: measurements, modeling, and interpretation, Journal of the Acoustical Society of America, vol. 127, no. 6, 2010.
4. R. van Vossen *et al.*, Low frequency synthetic aperture sonar system for the detection of objects buried in mud, Proc. UDT Europe. Alicante, Spain (May 2012).
5. P.T. Gough and D.W. Hawkins, A unified framework for modern synthetic aperture imaging algorithms, Journal of Imaging Systems and Tech, vol. 8, 1996.
6. H.J. Callow *et al.*, Motion compensation improvements for widebeam multiple transducer systems, IEEE Journal of Oceanic Engineering, no. 34, vol. 3, 2009.
7. M.P. Hayes and A.J. Hunter, Adaptive beamforming for low frequency SAS imagery and bathymetry, Proc. ECUA. Edinburgh, UK (Jul 2012).
8. A. Tesei *et al.*, At-sea measurements of acoustic elastic scattering by a 1.5 m long cylinder made of composite materials, Proc. UAM. Crete, Greece (2007).

Appendix D Tutorial for iSAAM Workshop, Dec 2012

iSAAM-2012: Tutorial on Ultra Low Frequency Wideband and Widebeam Sonar Processing

Alan Hunter

TNO (Netherlands Organisation for Applied Scientific Research)

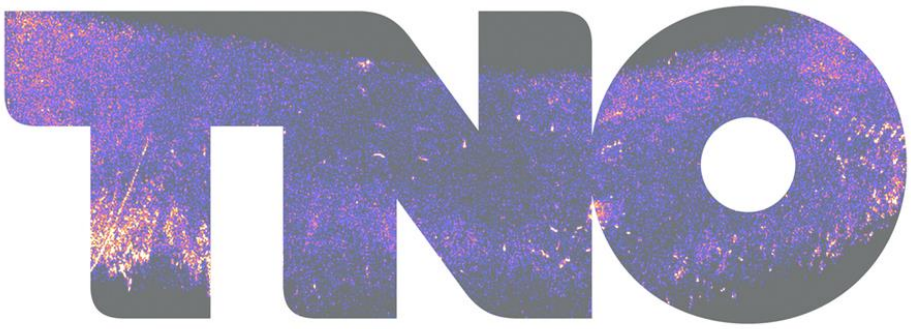

1.

iSAAM Workshop

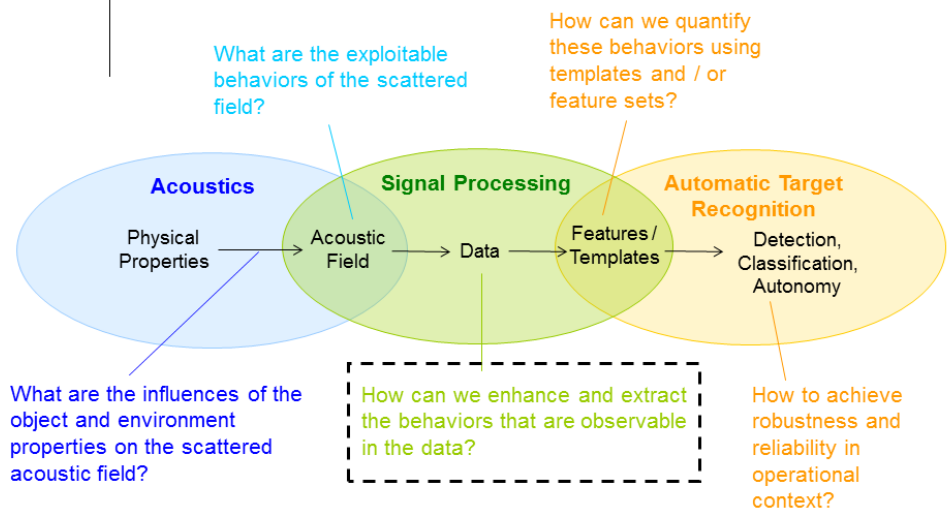

2.

Outline

- Definition & motivation
  - What is ultra low-frequency, wideband, widebeam sonar and why use it?
- Data pre-processing
  - Multipath suppression
  - SAS imaging
  - Widebeam motion compensation
- Target response isolation and interpretation
  - Background removal
  - Reverse SAS processing
  - Multi-aspect acoustic colour
- *Examples from TNO's sediment-penetrating sonar (MUD)*

3.

Ultra Low Frequency, Wideband

- A definition:
  - Range of wavelengths that are comparable to object dimensions
    → Elastic scattering regime
- Object dimensions ~ 30mm – 1.5m

$$\lambda = \frac{c}{f}$$

→ Frequencies ~ 1kHz – 50kHz

High Frequencies: Geometrical Scattering

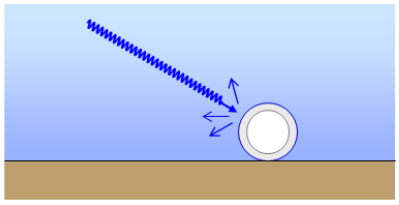

Low Frequencies: Elastic Scattering

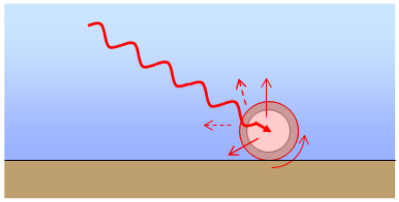

4.

Ultra Low Frequency, Wideband

"Ultra Low-Frequency"

$$f < 50\,\text{kHz}$$

"Ultra Wideband"

$$\frac{f_c}{\text{BW}} < 2$$

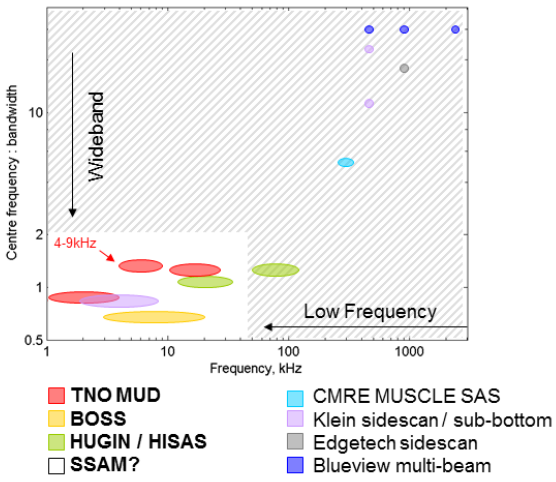

- TNO MUD
- BOSS
- HUGIN / HISAS
- SSAM?
- CMRE MUSCLE SAS
- Klein sidescan / sub-bottom
- Edgetech sidescan
- Blueview multi-beam

5.

Ultra Wide Beams

- Transducer beamwidth depends on frequency f and aperture size L

$$B(\theta, f) = \text{sinc}\left(\frac{L}{\lambda}\sin\theta\right)$$

$$\lambda = \frac{c}{f}$$

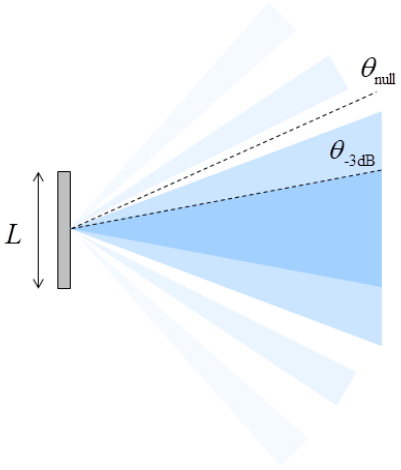

- For a constant aperture size, the beamwidth increases with decreasing frequency

6.

TNO innovation for life

Ultra Wide Beams

- Consequence of ultra low frequencies and physical size constraint on transducers
  →Wider beams
- Objects are illuminated over a range of angles
  - Ability to extract aspect-dependence information

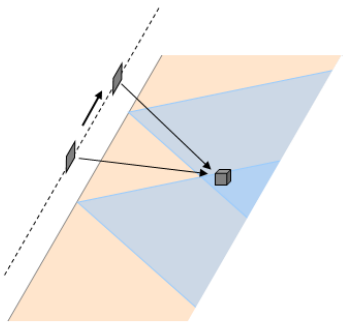

7.

TNO innovation for life

Ultra Low-Frequency, Wideband, Widebeam Sonar

"Ultra Low-Frequency"

$f < 50\,\mathrm{kHz}$

"Ultra Wideband"

$\frac{f_c}{\mathrm{BW}} < 2$

"Ultra Widebeam" (along-track)

$\theta \geq \pm 30\,\mathrm{deg}$?

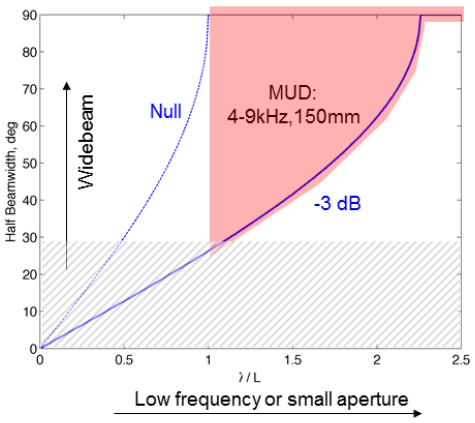

8.

TNO innovation for life

Why use Ultra Low Frequencies, Widebands, and Widebeams?

- Two reasons that affect operational capabilities, effectiveness, and efficiency:

1. The clutter problem
   - Inefficiency caused by need to identify false alarms
   - Practical limitation on "huntable" areas of seafloor

2. Buried objects
   - Limitation of capability to detect only proud / semi-buried objects

9.

Reason 1 – The Clutter Problem

- Benign versus complex seafloors
- Complex seafloor example
  - Approx. 50 detections in 50x50m
  - Optimistic 2% chance of misclassification
    → 1 FA → 400 / sq km !

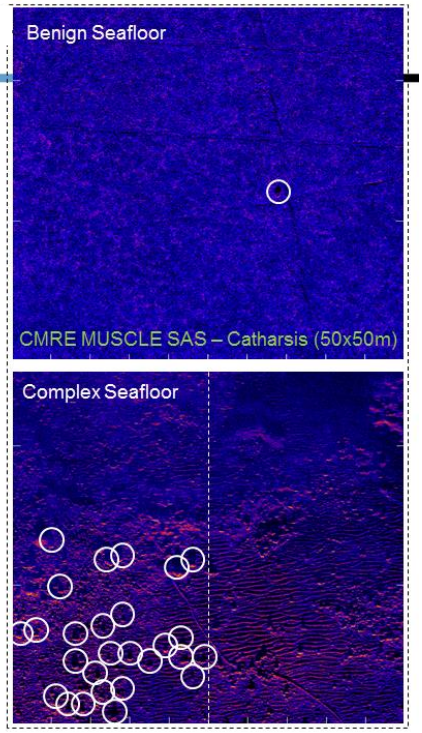

10.

Reason 1 – The Clutter Problem

- Operational effectiveness is very sensitive to ATR performance
  - HF high-resolution SAS is not always sufficient
  - Low frequencies
    - Object resonance
  - Wideband & widebeam
    - Frequency and aspect dependence

  → Object's external / internal structure and composition

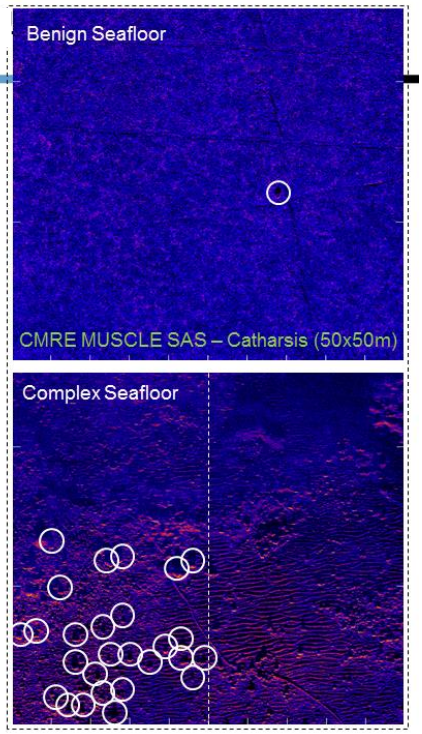

11.

TNO innovation for life

Reason 2 – Buried Object Detection

- Less absorption in the sediment at low frequencies
  - Sediment penetration → Buried object detection
- Favourable resonance-to-reverberation ratio
- Clutter is also a problem for buried objects (demonstrated later)

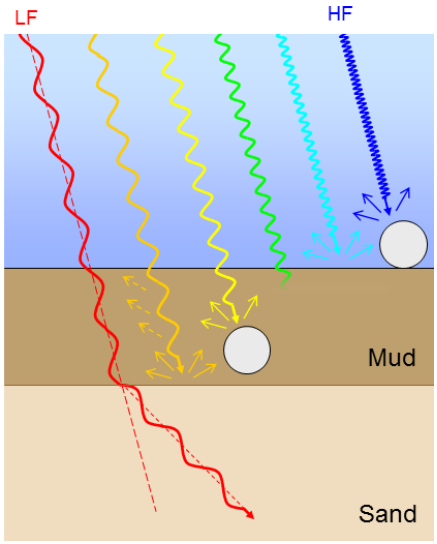

12.

TNO innovation for life

High versus Low-Frequency Classification

High Frequencies: Geometrical Scattering

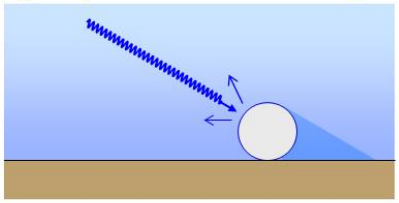

HF (CMRE MUSCLE SAS)

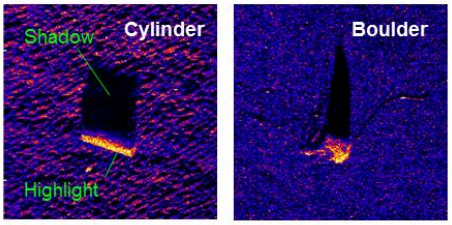

Low Frequencies: Penetration + Elastic Scattering

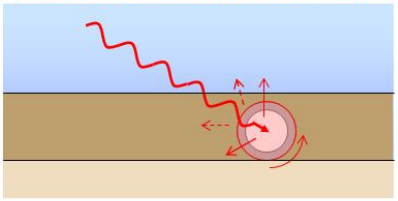

LF (TNO MUD SAS)

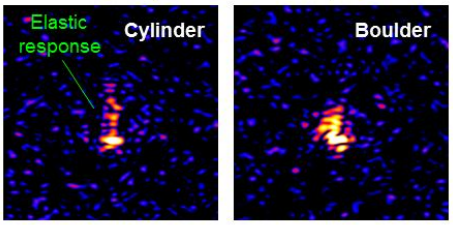

13.

TNO MUD System

- Detect objects buried in mud with high area coverage rate
  - Low-frequency sidescan sonar
  - Funding and support from Royal Netherlands Navy
  - Funding for acoustic colour analysis from SERDP
- MUD System
  - Hull-mounted frame
  - Vertical array: 16 elements
  - Sources: VLF* (1-4 kHz), **LF (4-9 kHz)**, HF (13-24kHz)
  - GPS and INS

* DGA / GESMA

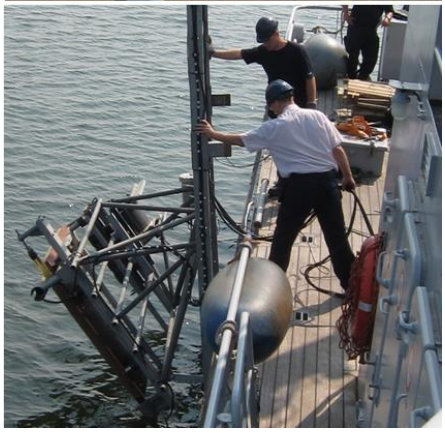

14.

MUD-2011 Trial

- Test garden – Haringvliet, Netherlands
  - Various objects deployed 6 months prior to trial
  - Active burial by divers
  - REMUS survey
  - 5 days; 200 runs
    - Different offsets and orientations

15.

Detection of Objects Buried in Mud

TNO innovation for life

Shells

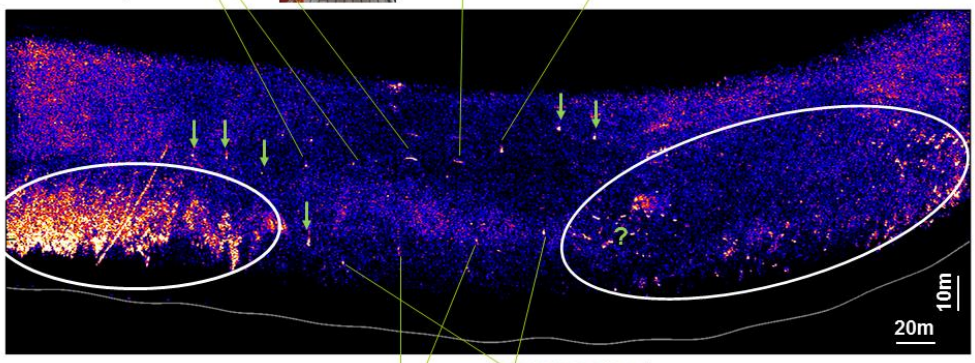

Bombs

16.

TNO innovation for life

Data Processing Chain

- Processing chain for an ultra low frequency (wideband & widebeam) sonar
  - Based on the TNO MUD System
  - For each stage, describe the purpose and implementation
- Examples using experimental data from the TNO MUD system

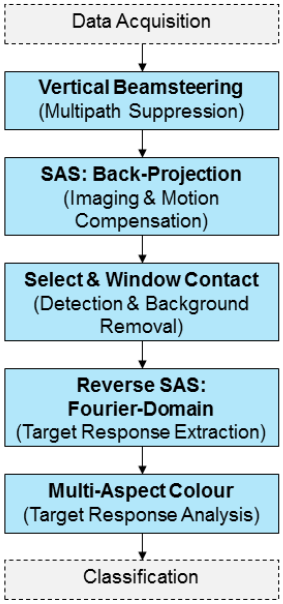

17.

TNO innovation for life

Data Processing Chain

- Vertical beamsteering
  - Relevant in shallow waters
  - TNO MUD trials: 10-15m water

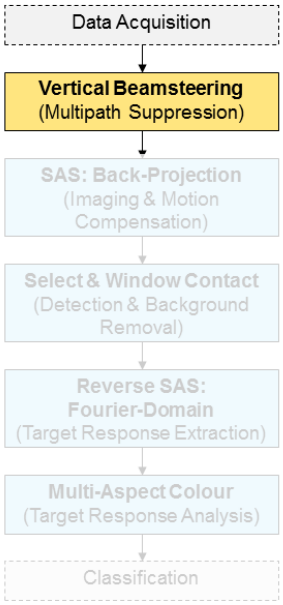

18.

Multipath in Shallow Water

- Multipath is a problem in shallow water and is exacerbated by using wide beams (i.e., at low frequencies)
- Reverberation and multipath can occlude the target response

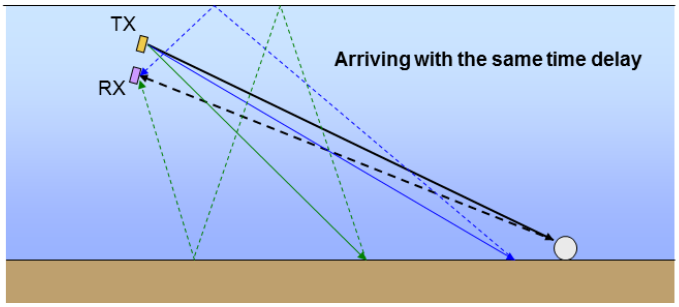

19.

Vertical Beamsteering for Multipath Suppression

- Vertical array of receiver elements
  - Sum signals → Narrow beam
  - Apply linear phase delays before summing → Steer beam
- Steer beam to points of interest on the seafloor, suppressing interference from multipath
- Low frequencies
  → Longer wavelengths
  → Need larger arrays

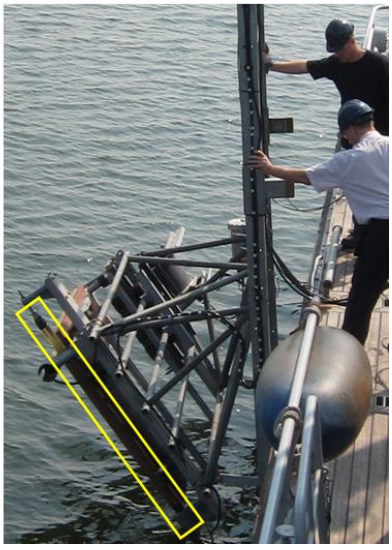

20.

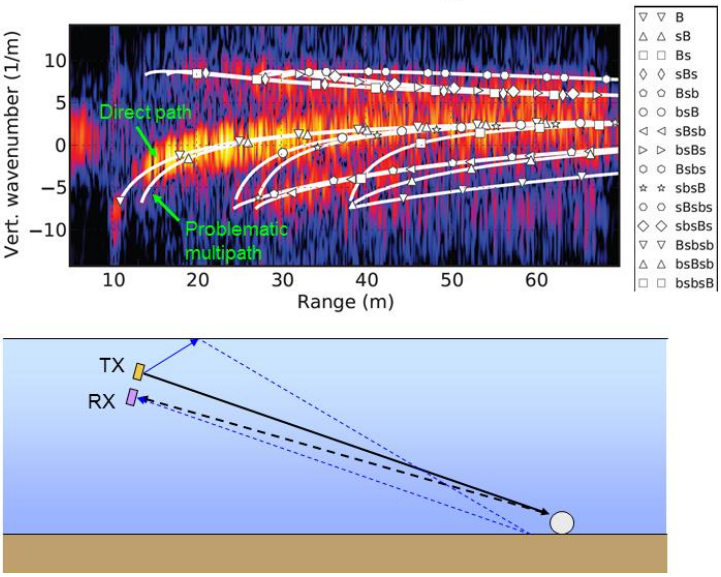
MUD – Vertical Beamsteering
Vert. wavenumber (1/m)
10
5
0
−5
−10
Direct path
Problematic multipath
10
20
30
40
50
60
Range (m)
B
sB
Bs
sBs
Bsb
bsB
sBsb
bsBs
Bsbs
sbsB
sBsbs
sbsBs
Bsbsb
bsBsb
bsbsB
TX
RX

21.

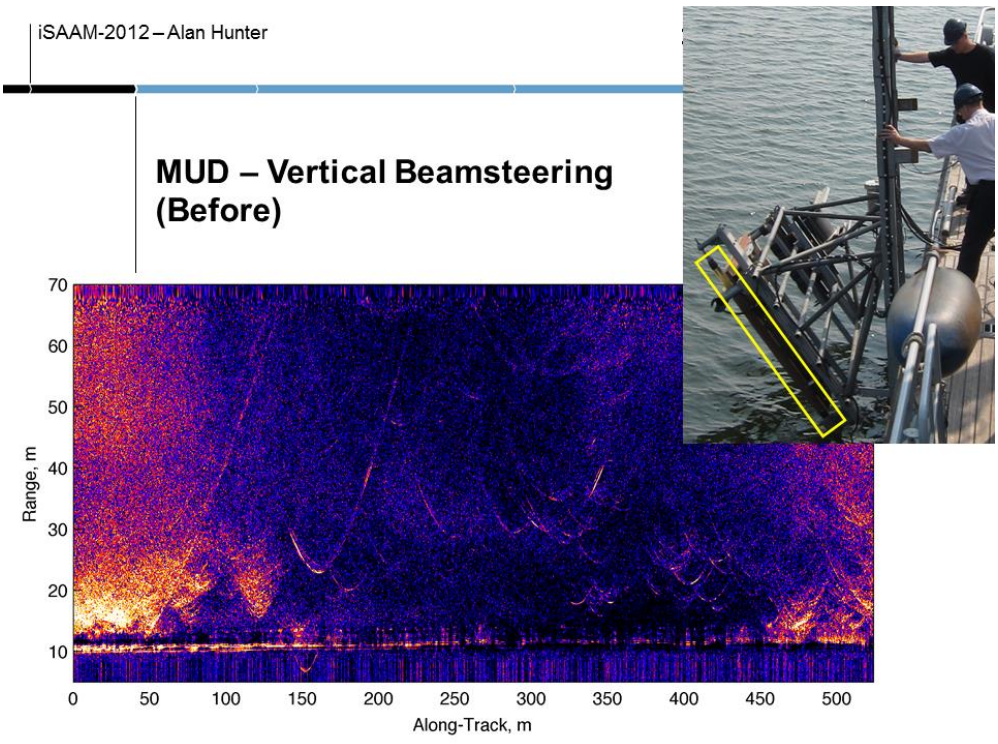
MUD – Vertical Beamsteering (Before)
Range, m
70
60
50
40
30
20
10
0
50
100
150
200
250
300
350
400
450
500
Along-Track, m

22.

MUD – Vertical Beamsteering (After)

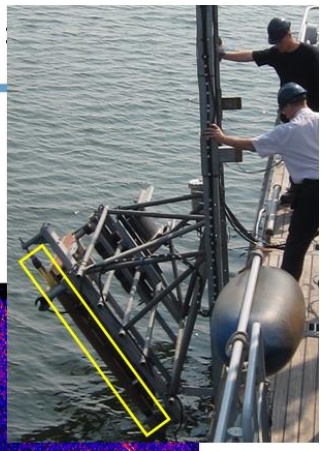

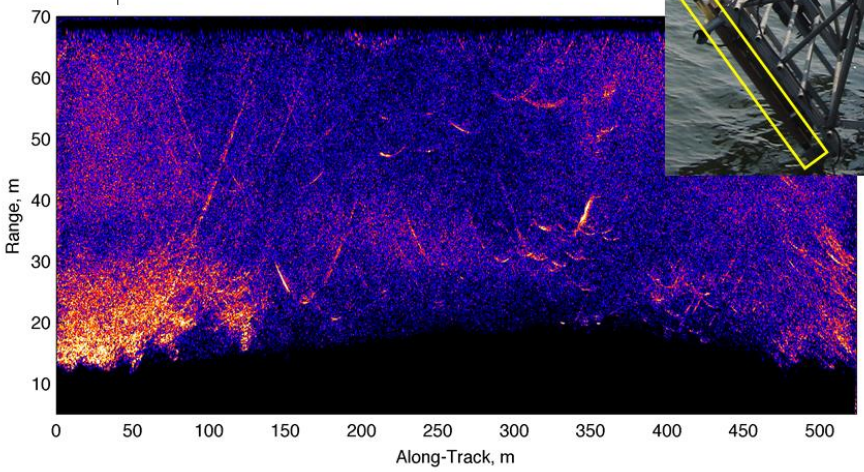

23.

TNO innovation for life

Data Processing Chain

- Synthetic aperture sonar (SAS) processing
  - Space/time domain: *Back-projection algorithm*
  - Fourier domain: *ω-k algorithm*

  SAS is essential for ultra low frequencies / widebeam

  Brief recap of principles

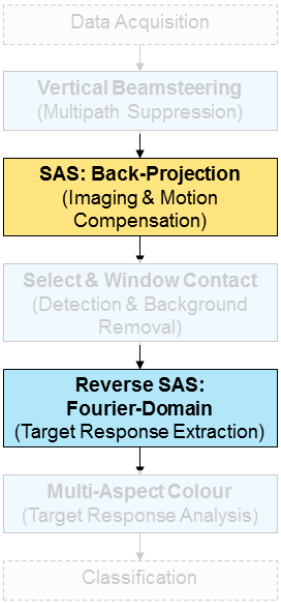

24.

Widebeam Sidescan Echo Data – Why is SAS essential?

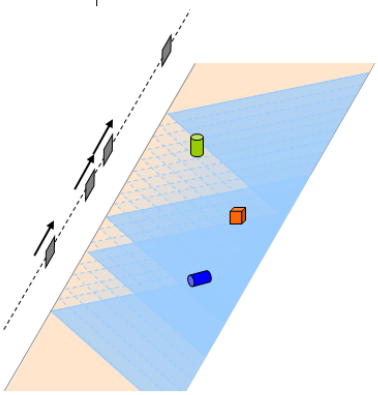

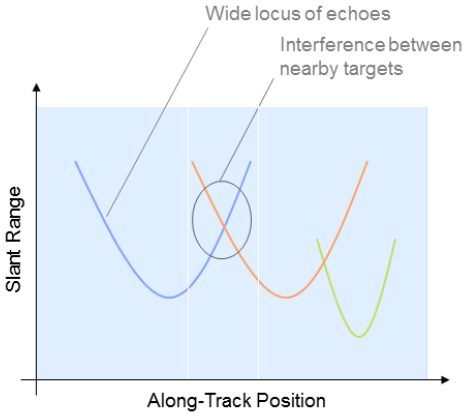

25.

SAS Imaging (Backprojection / Delay-and-Sum)

- For each image pixel, coherently integrate along locus of echoes

$$i(x,y \mid x_0,y_0,z_0) = \int d(u, 2r/c)\,\mathrm{d}u$$

$$r = \sqrt{(x-u)^2 + (y-y_{\text{sway}})^2 + (z-z_{\text{floor}})^2}$$

  - Coherent echoes sum constructively

→ Focusing & increased SNR

- Advantages & disadvantages
  + Simple implementation
  + Wide-beam motion compensation for arbitrary imaging geometries
  – Slow (but parallelisable)

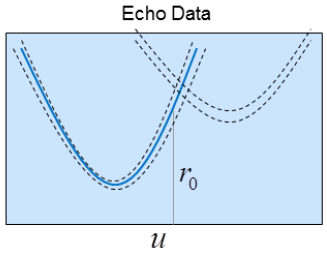

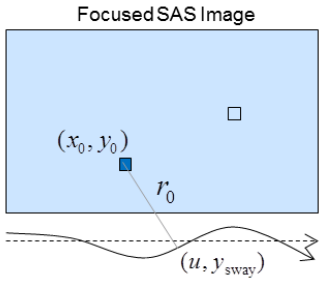

26.

TNO innovation for life

MUD – SAS Processing

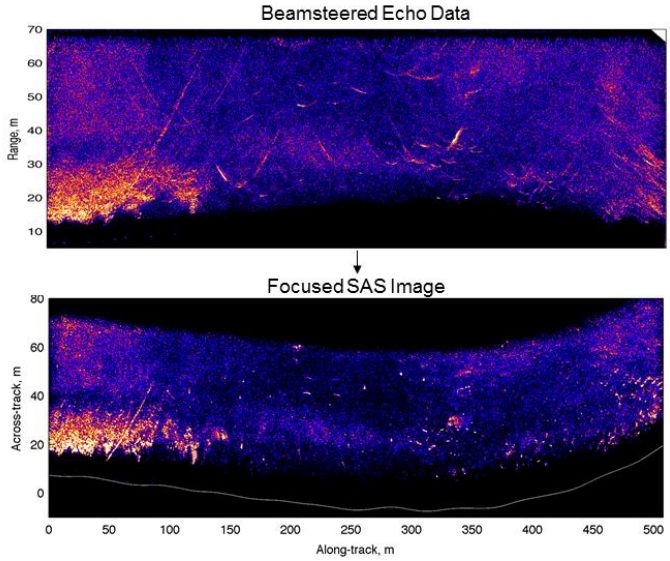

27.

Sensitivity to Motion Errors

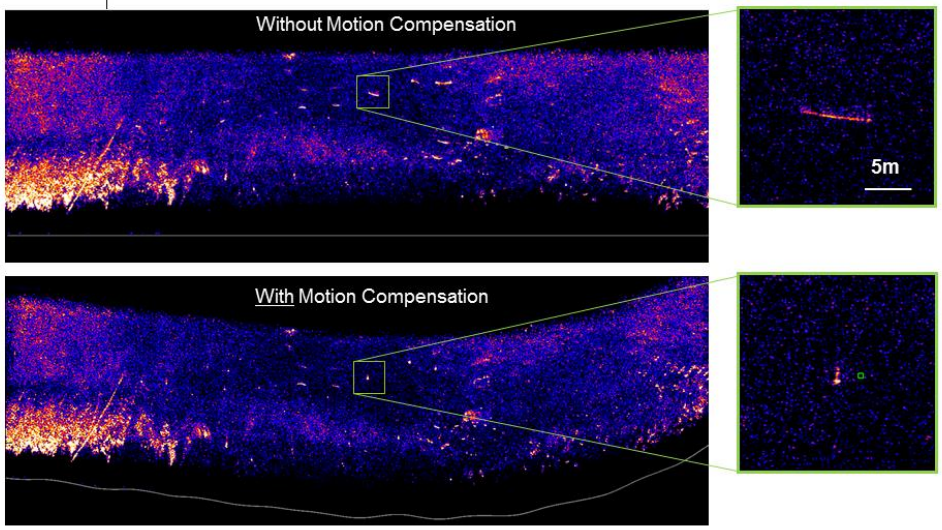

28.

TNO innovation for life

SAS Imaging (ω – k Algorithm)

- Fourier-domain implementation, assuming regular sampling
  - Simply a warping of the Fourier space via the Stolt mapping

$$I(k_x, k_y) = \text{Stolt}\{D(k_u, k)\}$$

$$\text{Stolt}: \begin{cases} k_x = k_u, \\ k_y = \sqrt{4k^2 - k_u^2} \end{cases}$$

- Advantages & disadvantages
  - Fast (Fourier transforms)
  - Wide-beam motion compensation is difficult
  - Easily reversed

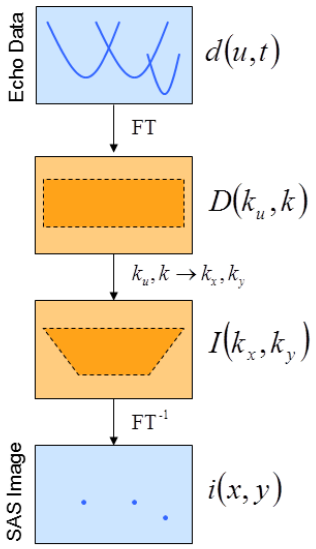

29.

TNO innovation for life

Data Processing Chain

- Select target of interest in the SAS image
- Separate it from the background and other nearby targets by windowing

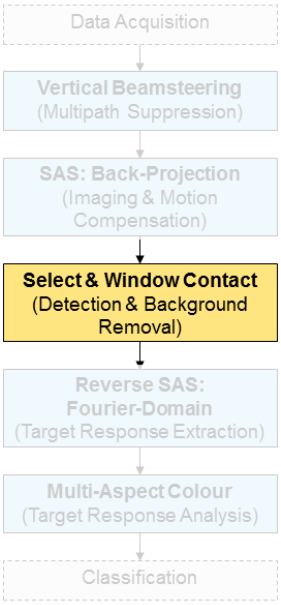

30.

Target Selection (Detection)

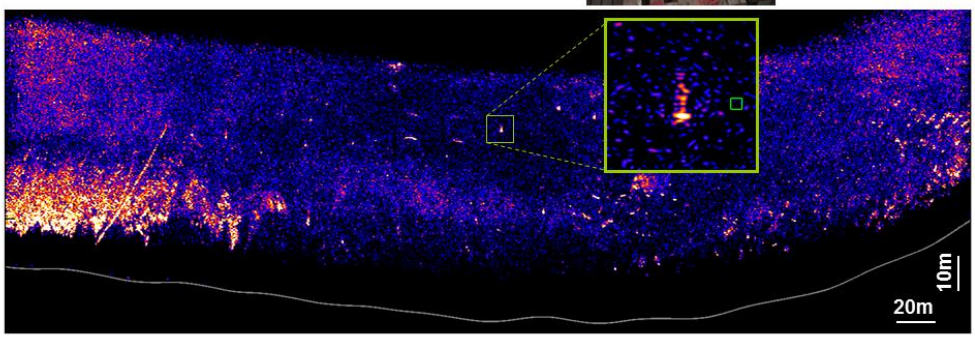

Isolation of Target from Background

- Targets can be resolved from one another in the SAS image
- Isolate target of interest by windowing, e.g.,

$$t'(x,y) = t(x,y)\,\mathrm{win}(x,y)$$
$$\mathrm{win}(x,y) = \mathrm{rect}(x/L_x, y/L_y)$$

- However, there is a trade-off for the choice of window size
- Currently working on a better solution for target / background separation

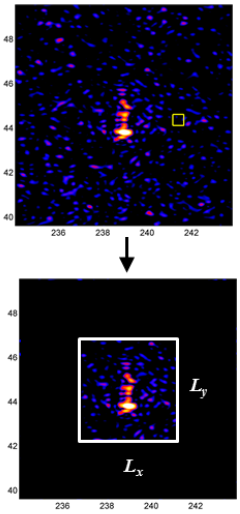

TNO innovation for life

Data Processing Chain

- Use reverse SAS processing to recover the target echo response

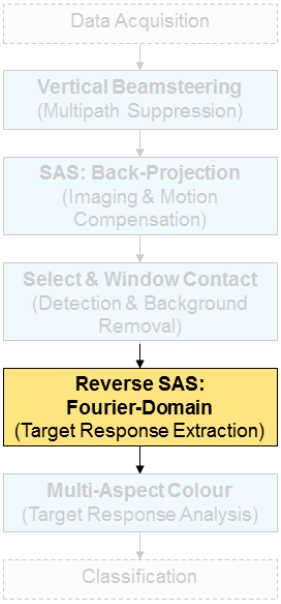

33.

TNO innovation for life

Reverse SAS Imaging

- ω-k algorithm is easily reversed
  - Stolt mapping converts from data to image
  - Inverse Stolt reverses this process

$$D(k_u,k)=\text{Stolt}^{-1}\{I(k_x,k_y)\}$$

$$\text{Stolt}^{-1}:\begin{cases}k_u=k_x,\\ k=\frac{1}{2}\sqrt{k_x^2+k_y^2}\end{cases}$$

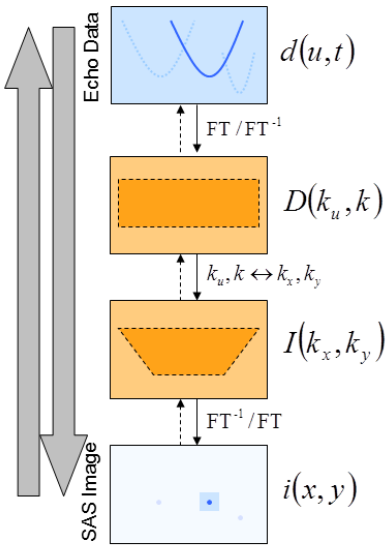

34.

TNO innovation for life

Target Echo Response

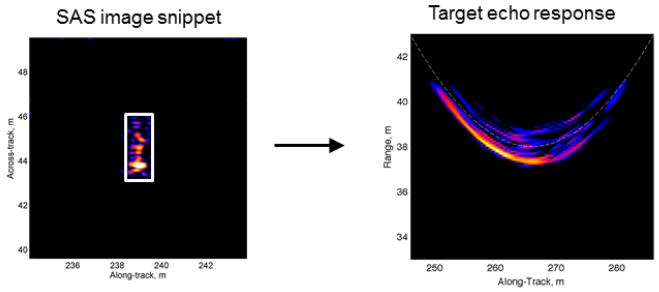

SAS, window, reverse SAS

35.

TNO innovation for life

Data Processing Chain

- Multi-aspect acoustic colour: information on frequency and aspect dependence of target scattering

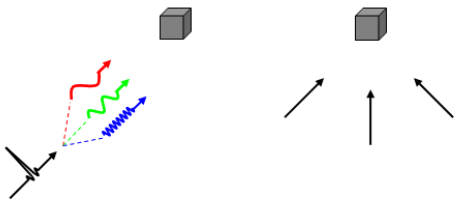

Data Acquisition

Vertical Beamsteering (Multipath Suppression)

SAS: Back-Projection (Imaging & Motion Compensation)

Select & Window Contact (Detection & Background Removal)

Reverse SAS: Fourier-Domain (Target Response Extraction)

Multi-Aspect Colour (Target Response Analysis)

Classification

36.

TNO innovation for life

Multi-Aspect Acoustic Colour

- Fourier transform of echo data in range → temporal wavenumber

$$k = \frac{2\pi f}{c}$$

- Fourier transform of echo data in along-track → wavenumber

$$k_u = k \sin\theta$$

- Multi-aspect acoustic colour mapping

$$f = kc / 2\pi$$
$$\theta = \sin^{-1}(k_u / k)$$

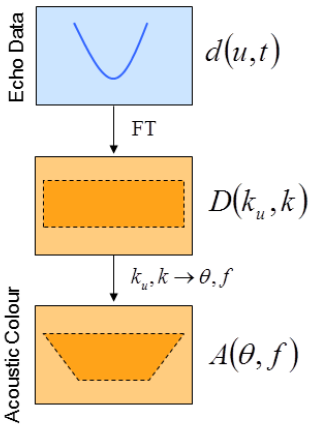

37.

TNO innovation for life

Multi-Aspect Acoustic Colour

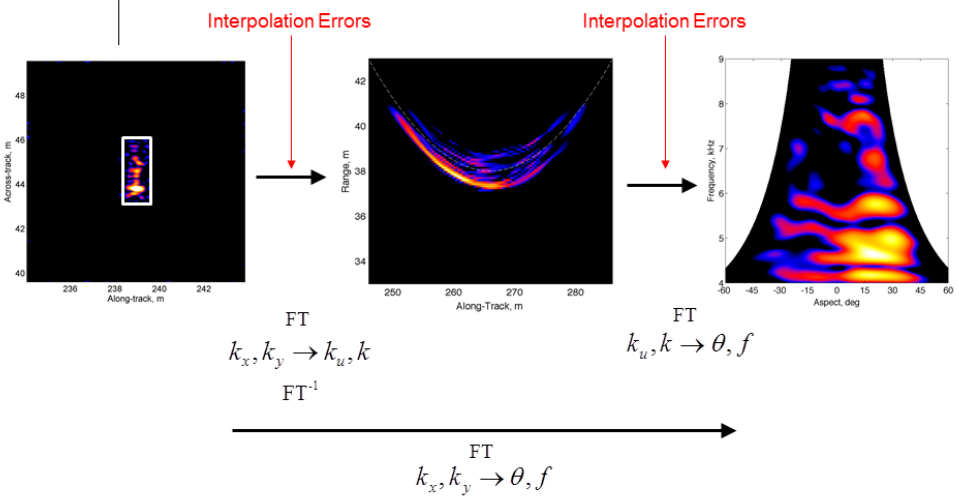

38.

Summary

- Cannot recover the target echo response directly from the data
  - SAS required
- All information on the target is contained within the SAS image snippet
- Different representations of the same data:
  - SAS image snippet
  - Target echo response
  - Multi-aspect acoustic colour

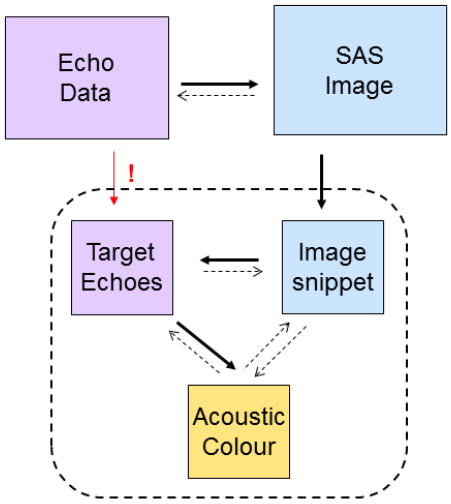

39.

Results and Discussion

- Results from our at-sea experiments with the MUD System
- Stimulate discussions …

40.

TNO innovation for life

MUD-2011 Results for CMRE EVA Cylinder

- 1.5m long, 0.5m diameter
- Thin-walled fibreglass shell
- Water-filled
- One end filled with Epoxy resin

41.

TNO innovation for life

CMRE EVA Cylinder – End-On, Long Range

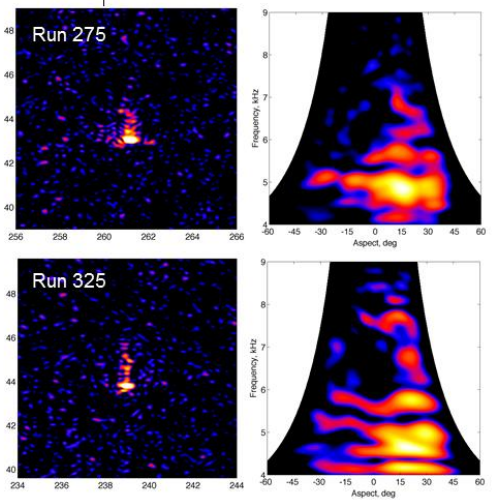

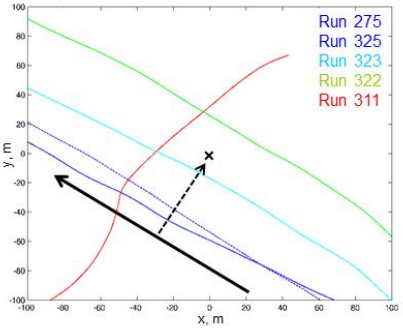

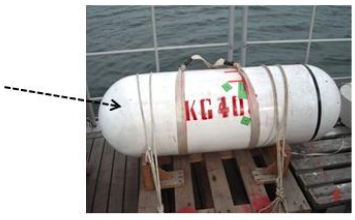

42.

CMRE EVA Cylinder – End-On

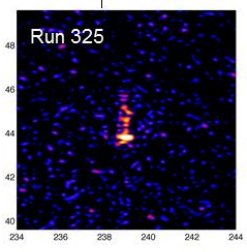

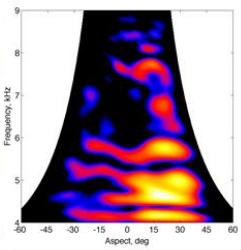

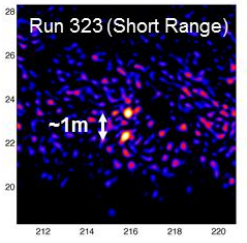

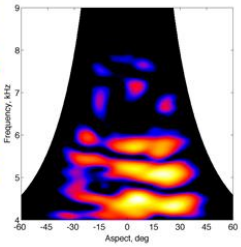

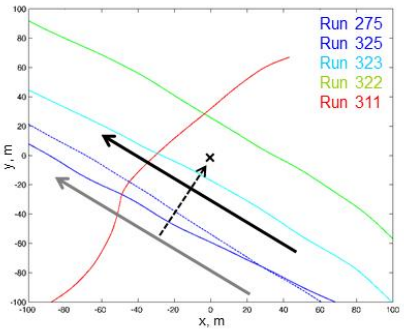

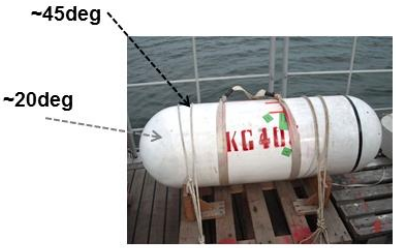

43.

CMRE EVA Cylinder – End-On, Opposite Sides

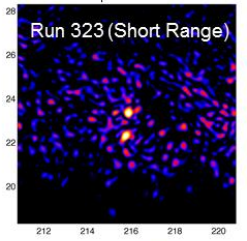

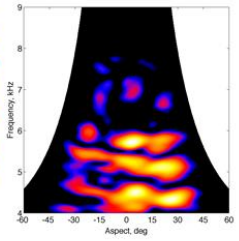

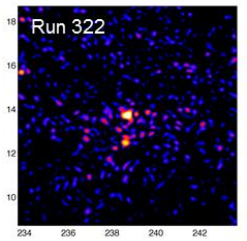

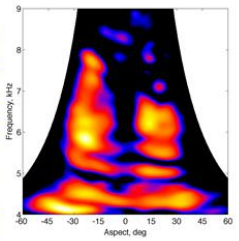

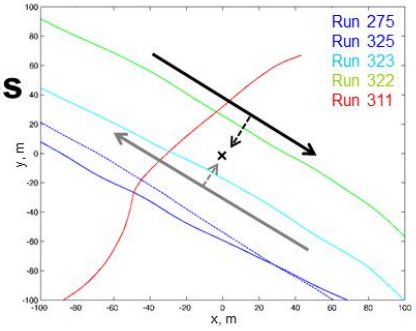

44.

TNO innovation for life

CMRE EVA Cylinder – Broadside, Short Range

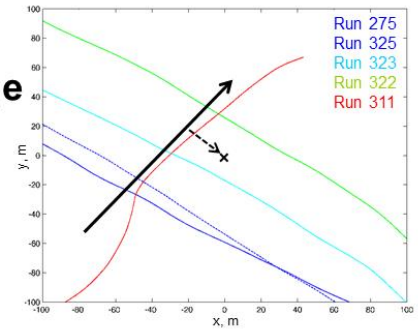

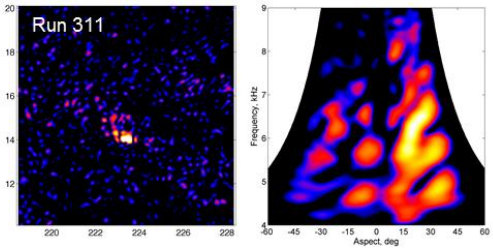

45.

TNO innovation for life

CMRE EVA Cylinder – Multi-View "Fusion"

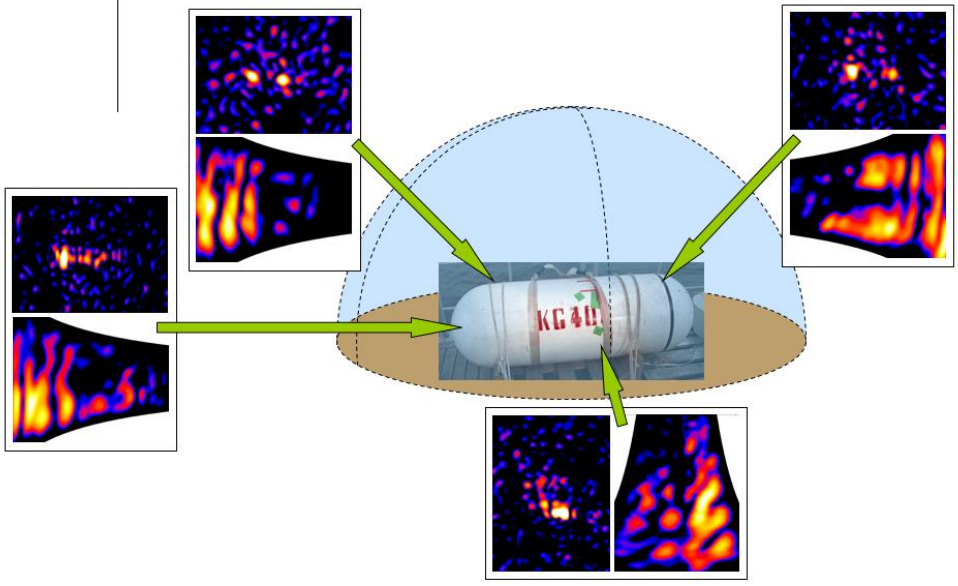

46.

Summary

- **Signal processing:**
  - Motivation for using ultra low freqnuecies, wideband & widebeams
  - Description of our processing chain (SAS is essential step for dealing with large echo loci; all info contained in SAS image snippet)
  - Demonstrated multi-aspect acoustic colour extraction on data from an experimental system in a realistic operational environment

- Where next?
  - **Signal processing:** Processing improvements; study more targets; assess the robustness
  - **Acoustics:** Validate and understand results by FE simulation
  - **ATR:** Investigate robust features

REPORT DOCUMENTATION PAGE

Form Approved
OMB No. 0704-0188

1. REPORT DATE *(DD-MM-YYYY)*	**2. REPORT TYPE**	**3. DATES COVERED** *(From - To)*

5. TITLE AND SUBTITLE

Final Report SERDP MR-2200: Detection of Underwater UXOs in Mud

5a. CONTRACT NUMBER

5b. GRANT NUMBER

5c. PROGRAM ELEMENT NUMBER

6. AUTHOR(S)

A.J. Hunter and R. van Vossen

5d. PROJECT NUMBER
SERDP MR-2200

5e. TASK NUMBER

5f. WORK UNIT NUMBER

7. PERFORMING ORGANIZATION NAME(S) AND ADDRESS(ES)

TNO (Netherlands Organisation for Applied Scientific Research)
Oude Waalsdorperweg 63
2597 AK, The Hague,
The Netherlands

8. PERFORMING ORGANIZATION REPORT NUMBER

9. SPONSORING / MONITORING AGENCY NAME(S) AND ADDRESS(ES)
SERDP

10. SPONSOR/MONITOR'S ACRONYM(S)

11. SPONSOR/MONITOR'S REPORT NUMBER(S)

12. DISTRIBUTION / AVAILABILITY STATEMENT

13. SUPPLEMENTARY NOTES

14. ABSTRACT

One of the most problematic areas where unexploded ordnance (UXO) can be situated is in an underwater environment, buried in sediment. Since burial frequently occurs in silt or mud, it is of great importance to have a capability for the detection of UXO in such buried conditions. This project considers detection of objects buried in mud using a side-looking low frequency (LF) sonar system mounted on a boat. The detection of buried UXO with a LF side-looking sonar system, however, is a challenging problem. This is primarily caused by high reverberation and possible clutter. In addition, the amplitude of the target echo of an object is reduced by burial. For these conditions, dedicated processing has to be developed for the detection of UXO and other targets of interest, and for the subsequent discrimination between targets and clutter contacts. In this project robust and advanced processing techniques are developed with the objective to improve detection and classification in operational conditions. These techniques have been demonstrated on experimental data.

15. SUBJECT TERMS

16. SECURITY CLASSIFICATION OF:			**17. LIMITATION OF ABSTRACT**	**18. NUMBER OF PAGES**	**19a. NAME OF RESPONSIBLE PERSON**
a. REPORT	**b. ABSTRACT**	**c. THIS PAGE**			**19b. TELEPHONE NUMBER** *(include area code)*